Master's thesis

NTNU
Norwegian University of Science and Technology
Faculty of Natural Sciences
Department of Chemistry

Sigurd Norum Botten

Developing synthesis route for CuSAPO-18

Master's thesis in MSCHEM
Supervisor: Karina Mathisen
May 2019

NTNU
Norwegian University of
Science and Technology

Sigurd Norum Botten

Devoling synthesis route for CuSAPO-18

Master's thesis in MSCHEM
Supervisor: Karina Mathisen
May 2019

Norwegian University of Science and Technology
Faculty of Natural Sciences
Department of Chemistry

NTNU
Kunnskap for en bedre verden

Acknowledgements

This work was performed at the Department of Chemistry at the Norwegian University of Science and Technology (NTNU). The first and largest thanks goes my supervisor Dr. Karina Mathisen and co-supervisor Guro Sørli, both of whom have provided invaluable help, guidance, and feedback throughout the process.

Thanks are also extended to Kristin Høydalsvik Wells and Silje Marie Dale for assistance with XRD, Laura Rioja-Monllor for assistance with BET, Syverin Lierhagen with ICP-MS, Daniel Ali with FT-IR, and Guro Sørli for assistance with catalysis.

I would also like to thank the other members of the structural chemistry group, both for fruitful discussions and for making the time spend –both in the lab, in our meetings, and in our social events– thoroughly enjoyable. I would also like to thank the other students at the department with whom I have made acquaintance, or better yet friendship, and who have helped make the time spend unforgettable.

Abstract

In the present work the synthesis of SAPO-18 with copper isomorphously substituted is attempted by hydrothermal method. Methods using di-isopropylethylamine (DIPEA) was found to reduce some or all of the copper to metal. Therefore a modified version of the method of Wendelbo et al.[1] which uses tetraethylaminehydroxide (TEAOH) was developed. Lower water content of the gel was found to be critical to this synthesis.

A copper containing sample using such a method was synthesised. This sample was investigated using XRD, BET, ICP-MS and FT-IR. Unfortunately the exact nature of copper in this sample could not be determined. Lowering the amount of tetraethylaminehydroxide was key to obtaining this sample. Same sample was found to be less active for the selective catalytic reduction (HC-SCR) of NO_x that a sample with copper introduced via ion-exchange.

Sammendrag

I dette arbeidet ble synthese av SAPO-18 med kobber isomorfisk substituert forsøkt via en hydrotermisk metode. Metoder basert på di-isopropyletylamin (DIPEA) ble funnet til å redusere deler av eller alt kobberet til metallisk. Derfor ble en modifisert version av metoden til Wendelbo et al.[1] som bruker tetraetylaminhydroksid (TEAOH) utviklet. Lavere vanninnhold i gelen ble funnet til å være kritisk for denne syntesen.

En kobberholding prøve ble syntetisert via slik metode. Denne prøven ble analysert ved hjelp av XRD, BET, ICP-MS, og FT-IR. Desverre kunne ikke den eksakte tilstanden til kobber etableres. Å senke mengden tetraetylaminhydroksid var essensielt for å danne denne prøven. Samme prøve ble funnet til å være mindre aktiv i selektiv katalytisk reduksjon (HC-SCR) av NO_x enn prøver med kobber introdusert via ionebytting.

Abbreviations

AEI	Structure code for topology of $AlPO_4$-18.
AFI	Structure code for topology of $AlPO_4$-5.
AFR	Structure code for topology of $AlPO_4$-40
Al_2O_3	Aluminium oxide (alumina)
AlO(OH)	Pseudobohemite
BET	Brunauer-Emmett-Teller
calc.	Calcined
CHA	Structure code for topology of chabazite.
CO	Carbon monoxide
Cu	Copper
CuO	Copper oxide
$CuSO_4 \cdot H_2O$	Coppersulfate monohydrate
D6R	Double 6-Ring
DIPEA	*N*-*N*-Diisopropylethylamine
EtOH	Ethanol
FT-IR	Fourier-Transform InfraRed spectroscopy
HAc	Acetic acid
HC-SCR	Selective catalytic reduction with hydrocarbons
H_2O	Water
H_3PO_4	Phosphoric acid
ICP-MS	Inductively Coupled Plasma Mass Spectroscopy
MFC	Mass Flow Controller
NH_3	Ammonia
NH_4NO_3	Ammonium nitrate
NO_x	Nitrogen oxide and Nitric oxide
O	Oxygen
P	Phosphorous
PEG	Polyethylene glycol
SCR	Selective catalytic reduction
SFR	Stacking Fault Rate

SNS	Supernatant Solution
Si	Silicon
SiO_2	Silicon oxide (silica)
TEAOH	Tetraethylamine hydroxide
TEPA	Tetraethylpentaamine
TMAOH	Tetramethylamine hydroxide
TPAOH	Tetrapropylamine hydroxide
XRD	X-Ray Diffraction

Contents

Chapter 1

Motivation

Microporous aluminiumphosphates (AlPO's) are a class of zeotypes discovered by Wilson et al.[2] Rapidly after their first synthesis, numerous other elements, especially Si and transition metals, have been incorporated in such materials.[3–5] Aluminiumphosphates are, alike other zeotypes and zeolites, noted for their high surface areas, high thermal stabilities, and their molecular sieve capabilities. By including other elements additional properties, including acidic sites, can be obtained.

Among such materials the Si substituted SAPO-18 is a promising candidate as a catalyst, though less studied than the related SAPO-34 material. This in contrast to the non-substituted materials where AlPO-18 is more studied than SAPO-34.[6] The cages in the SAPO-18 materials have different shape to the SAPO-34 ones and could allow for somewhat larger intermediates to form, and SAPO-18 has therefore been investigated as a catalyst for a variety of reactions, including methanol-to-olefin conversion,[7–9] dimethyl ether synthesis,[10] and to gas separation.[11]

Several works report inclusion of copper in SAPO-18 materials as well as the application of such, most commonly to the selective catalytic reduction of NO_x[11–13] but also other reactions like methanol to dimethylcarbonate.[14] However despite efforts to make such, to the author's best knowledge copper isomorphously substituted into SAPO-18 has not been reported.

The reduction of NO_x gasses is of particular interest as those gasses comprise a major pollutant, being associated with both respiratory and cardiovascular diseases[15] as well as with acid rain.[16] While lightning accounts for a natural source of NO_x, combustion engines account for a major part of human contributed NO_x.[17] Emitted NO_x has been on the decrease following deliberate efforts,[17] however in view of the Volkwagen scandal of 2015 it is clear that more research

is required towards the reduction of NO_x emissions.

Therefore the present work has attempted the synthesis of SAPO-18 with copper incorporated isomorphously into the framework for use as a catalyst in selective catalytic reduction of NO_x using propene.

Chapter 2

Theory

In this chapter the nature and properties of SAPO's is presented as well as methods for the inclusion of copper into SAPO materials. Structure and nature of SAPO-18 specifically is also presented. The nature of hierarchical materials is briefly given as well as the principle of characterization techniques used herein. Lastly theory for the selective catalytic reduction of NO_x is given.

2.1 SAPO's

The structures of zeotypes can be described by cornersharing TO_4 (T=Al, Si, P, Metal, etc.) tetrahedra, which build up rings and cages. Depending on the number of tetrahedra which build up each ring (denoted NR where N is the number of tetrahedra; such as 8R for eight-membered rings) the opening has a different diameter. The pore diameter (from its ring size and shape) and the interconnectivity of the pores are important characteristics of a given zeotype structure. As of time of writing 245 unique structures are verified.[18]

Aluminiumphosphates (AlPO-n) are a family of zeotypes consisting of strictly alternating Al and P as T atoms giving a charge neutral framework. SAPO-n are an extension of these where Si substitutes some T atoms. Two mechanisms have been proposed for the incorporation of Si in SAPO's.[3,19,20] Either one Si substitutes a P atom with the resultant negative charge being compensated by a Brønsted site on the resulting Si–(OH)–Al bridge ($OH_O^\bullet$):

$$SiO_2 \xrightarrow{AlPO_4} Si_P^{'} + Al_{Al}^{\times} + 3\,O_O^{\times} + OH_O^{\bullet} \tag{2.1}$$

or a pair of Si substitutes a neighbouring pair of Al and P:

$$2SiO_2 \xrightarrow{AlPO_4} Si_P^{'} + Si_{Al}^{\bullet} + 4\,O_O^{\times} \tag{2.2}$$

This does not result in a Brønsted site. However due to the instability of the Si–O–P bridge,[19] multiple neighbouring pairs are often replaced giving patches (or islands) of silica in the material. Such patches give rise to a disproportionally high number of surface Si–OH groups and possess slightly larger crystallographic lattice parameters.[21]

The synthesis of zeotypes typically is performed by a hydrothermal method[22] in the presence of an organic template (generally an amine) which ensures crystallization of a specific zeotype phase. These organics are then removed by thermal treatment (calcination) at ∼500 °C. The mechanism for this crystallization is still unresolved, and difficult to investigate due to the pressures and temperatures involved, the mixture of liquid and solid phases, and the vast number species present for any one system.[23,24] The synthesis gels used for SAPO's are typically weakly acidic,[23] while pH increases over crystallization.[25]

2.2 Copper functionalization in SAPO's

Various metals including copper can be included in a zeotype material.[26] This is primarily performed via one of three methods; impregnation, ion-exchange, and incorporation (in-synthesis). Impregnation refers to methods where a solution of precursor is reduced or precipitated in the presence of the support. Precipitation is typically achieved by heating the solution or by co-precipitation, i.e. mixing two precursors to form a insoluble salt. It will generally lead to the formation of particles in the nano- to micrometer range distributed on the surface of the support.[27–29] Ion-exchange refers to methods where pre-synthesised zeotype is exposed to dissolved cations which replace H^+-ions in Brønsted acid sites (See Figure 2.1 **C**).[30,31] Typically ion-exchange causes a substantial loss of surface area and crystallinity,[32,33] however by first exchanging with ammonium these can be preserved.[34,35]

Incorporation will generally refer to methods where cations are included in the synthesis and thus becomes part of the material. With these methods the cations are in two main kinds of sites; framework and extra-framework.

Framework incorporation as it is used in this work means isomorphous substitution of metal ion as a T atom in the structure. Extra-framework then includes, but is not limited to, being bound to Brønsted acid sites similar to that obtained by ion-exchange, loose complexes in the pores, or partially incorporated, i.e. partially bonded to framework atoms and partially to other ligands (such as H_2O). For many metals framework incorporation is obtainable by simply including a respective metal salt in the synthesis mixture.[7] However due to Cu^{2+}'s reducibility and preferred coordination (see Below) such methods give highly variant results.[36–38]

Hypothetically framework substitution of Cu^{2+} occurs as:

$$\mathrm{CuO} \xrightarrow{\mathrm{AlPO_4}} \mathrm{Cu}'_{\mathrm{Al}} + \mathrm{P}^{\times}_{\mathrm{P}} + 3\,\mathrm{O}^{\times}_{\mathrm{O}} + \mathrm{OH}^{\bullet}_{\mathrm{O}} \tag{2.3}$$

with formed $\mathrm{OH}^{\bullet}_{\mathrm{O}}$ which are distinct from those obtained by Si-substitution. The acid strength of Brønsted acid groups arising from framework substituted metal is typically lower than for groups arising from Si substitution.[7,21] Such substituted copper have a tetrahedral coordination. What colour such copper would give is not established as the colour also depends on ligands and oxidation state.[39,75] Nicholson and Nilsen[40] suggests Cu^{2+}'s preference for a distorted octahedral environment causes framework incorporation to result in a distortion around Cu^{2+} such that it is coordinated to 6 framework oxygen in a tetragonally distorted octahedral orientation. They reported such materials to transform from turquoise to grey upon calcination. However in group efforts[38,41–43] have consistently shown that copper incorporation into SAPO's give a blue product which becomes green upon calcination. Copper have in these works had an tetragonally distorted octahedral coordination.

At high temperatures (>190 °C) and in the presence of tertiary amines, Cu^{II} is reported[25] to first autoreduce to Cu^{I} then disproportionate to Cu^{II} and metallic copper;

$$\mathrm{Cu^{II}} \rightleftharpoons \mathrm{Cu^{I}} \longrightarrow \mathrm{Cu^{0}} + \mathrm{Cu^{II}} \tag{2.4}$$

The autoreduction to Cu^{I} occurs due to low stabilisation (by hydratisation) of Cu^{II}. Other factors such as available ligands and pH also affect the stability of these ions. In particular Cu^{2+} precipitates at basic pH.[25,44] The full nature of copper chemistry under hydrothermal condition is not well established, in part due to the high temperatures in question.

Efforts to incorporate Cu^{2+} into SAPO's by using a complexing agent (such as TEPA,[11,12,45,46] N,N'-bis(2-aminoethyl)-1,3-propanediamine[47]) are numerous. However while such complexes prevent the reduction of copper, Martínez-Franco et al.[12] found the Cu^{2+}-TEPA complex to still be present in as prepared samples, indicating that they prevent the incorporation of copper into the framework.

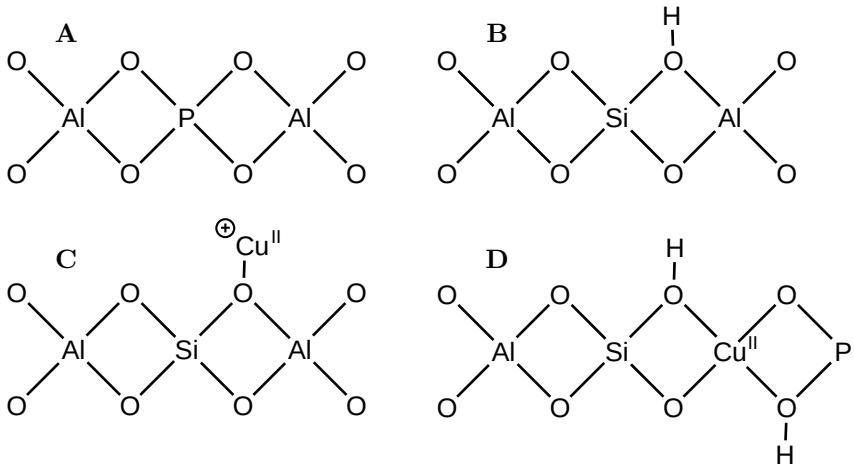

Figure 2.1: Simplified structures of different cases: **A** Unsubstituted AlPO. **B** P $\longrightarrow$ Si substitution in SAPO. **C** Extra framework Cu^{2+} in SAPO. **D** Al $\longrightarrow$ Cu substitution in CuSAPO. Any extraframework ligands or framework distortion as a result of Cu is omitted. Cu location is not coupled to Si location.

2.3 SAPO-18

SAPO-18 was first reported by Chen et al.[48] in 1994. Its structure, designated AEI (Figure 2.2), is closely related to that of SAPO-34 (Chabazite; CHA), differing only in the relative orientation of the double 6-ring building blocks (D6R). The pore system then is a similar 3D-interconnected network of 8R channels (3.8 Å × 3.8 Å)[49] with cavities that are greater than the channel openings. Notably the pear-shaped cages of AEI has a wider maximum than the cylindrical cages of the CHA structure.[50] The AEI cages would therefore allow a larger species to exist in the cage, which could be relevant to catalytic performance.

The AEI and CHA structures can be treated as stacks of layers of D6R rings with to different layer types; A and B, where the A and B layers are related by a 2_1 screw axis.[52] Ordered stacking of similar layers (AAAA or BBBB) give the CHA structure, while ordered stacking of alternating layers (ABAB) give the AEI structure. Unordered stacking give a structure referred to as AEI/CHA intergrowth.[53] It can be further described by a Stacking Fault Rate (SFR) which is the rate at which stacking switched from one type to another.[54] An SFR of 0 and 1 corresponds to CHA and AEI type materials respectively. Sławiński et al.[54] modelled how X-ray diffraction (XRD; see Section 2.5.1) patterns vary with SFR.

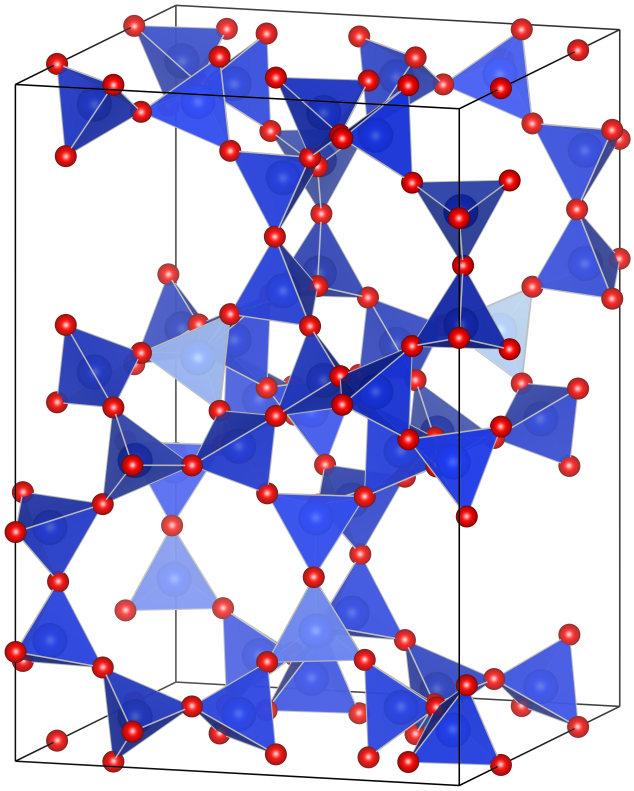

Figure 2.2: Unit cell of the AEI structure, showing T atoms (Al, Si, P) as blue and O as red. Rendered using the VESTA software[51] package.

The unordered stacking is obtained through two kinds of faults; *displacement* where a single layer of the alternate type is inserted (e.g. AAABAA) or *growth* where the layer type switches (e.g. AAABBB).

Initial synthesis[48] of SAPO-18 used di-isopropyletylamine (DIPEA; see Figure 2.4), which had not previously been reported used in zeotype synthesis. That work concluded that SAPO-18 could not be made using parameters adapted from AlPO-18 synthesis as this lead to formation of SAPO-34. However work by Wendelbo et al.[1] showed that by changing synthesis parameters SAPO-18 could be made using tetraetylammonium hydroxide (TEAOH; see Figure 2.4). Use of DIPEA is still dominant in the literature for SAPO-18 synthesis.

Wendelbo et al.[1] reported SAPO-18 synthesis at a low Si ratios (0.07) by redu-

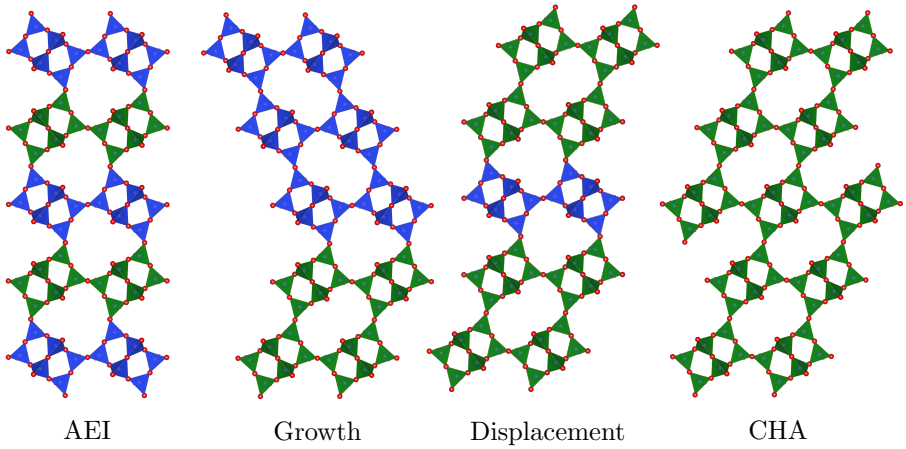

Figure 2.3: Stacking of D6R layers. Green tetrahedra corresponds to A type and blue to B type layers respectively, see text.

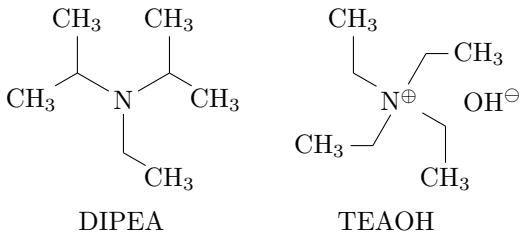

Figure 2.4: Chemical structure of DIPEA and TEAOH

cing the H_2O/Al_2O_3 ratio from 60 to 41. Smith et al.[53] reported transition from intergrowth to SAPO-18 when reducing the SiO_2 content. Wang et al.[9] similarly obtained SAPO-18 by varying the TEAOH/Al_2O_3 molar ratio between 1 and 2.4, obtaining SAPO-18 between 1.4 and 1.8. However due to differences in other parameters; such as H_3PO_4 content, synthesis order, and oxide sources (aluminiumisopropoxide v. bohemite etc.) there is limited transferability between the works.

Martínez-Franco et al.[12] reported synthesis of a Cu-SAPO-18 material by combining DIPEA with a polyamine which they complexed with the Cu^{2+} ions. In such materials the copper was found to be extra-framework similar to that obtained by ion-exchange. Turrina et al.[47] similarly reported using a polyamine

to complex Cu^{2+} (or Ni^{2+}), but using TEAOH as the templating agent. They found that by varying which polyamine and which of Ni^{2+} and Cu^{2+} was used, either SAPO-18 or SAPO-34 was formed. These results show that the inclusion of polyamines also affect the zeotype formed.

2.4 Hierarchical SAPO's

While the small pores of SAPO-18 and other zeotypes allow for high size and shape selectivity, the diffusion of species is limited. This in turn means only the outermost volumes of the particles are effectively available to such species. To mitigate this, mesopores (pores with diameter between 2 and 50 nm)[55] could be introduced into the material. Such mesopores, having much greater diameter, has less restriction of the transport of species through them.[56] Materials with connected pore systems in both the micro (<2 nm)[55] and meso range are labeled hierarchical. However for full utility such meso pores need to form an interconnected network throughout the material and to the particle surface so that they lower the effective diffusion distance for diffusing species.[56]

Synthesis of hierarchical zeotypes (or zeolites) is typically performed by templating[56] with either a solid or supramolecular template. Solid templates includes using carbon particles or polymers among others, which are encapsulated in the zeotype as it grows and removed afterwards. Supremolecular templating includes the use of surfactants which affect the surface of during crystallization. Notably both these techniques can cause formation of nanosized zeotype crystals instead. Of interest to this work is that the use of polyethylene glycol (PEG), which is a "solid" template, has been reported[8] to give hierarchical SAPO-18.

2.5 Characterization Methods

2.5.1 XRD

X-Ray Diffraction (XRD) is a powerful technique for determining the crystal structure of a material. In this method incident light at a specific wavelength is set at an angle, θ, to the material and only light reflected at the mirrored angle is measured (See Figure 2.5). From this it can be shown that constructive interference is obtained when Bragg's Law is fulfilled:

$$n\lambda = d \sin\theta \tag{2.5}$$

where n is a positive integer, λ is the wavelength, d is the distance between diffracting planes, and θ is the incident angle (See Figure 2.5). By convention 2θ is used as the experimental variable.

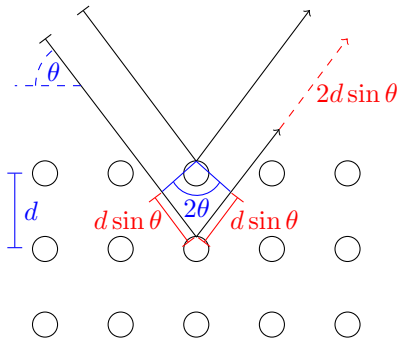

Figure 2.5: Illustration of the working principle of XRD.

The principle information obtained from XRD is the crystalline structure of the material; meaning which crystal phases are present (by their unique pattern) and to what extent it is present (by the height of peaks). A key limitation of XRD is its inability to detect particles of size less than 2–2.5 nm,[57,58] and it is thus unable to detect particles which are small enough to be encapsulated by zeolite cages.

In this work, XRD will be used to confirm SAPO-18 formation by comparing with the AEI pattern. Presence of competing phases (CHA, AFI, tridymite) are similarly identified. SFR will also be estimated from the XRD pattern. Additionally, presence of undesired copper phases is identified by the comparison with the patterns of metallic copper and tenorite (CuO) formed from the reduction of copper and oxidation of such metallic copper respectively. These patterns are given Figure 2.6.

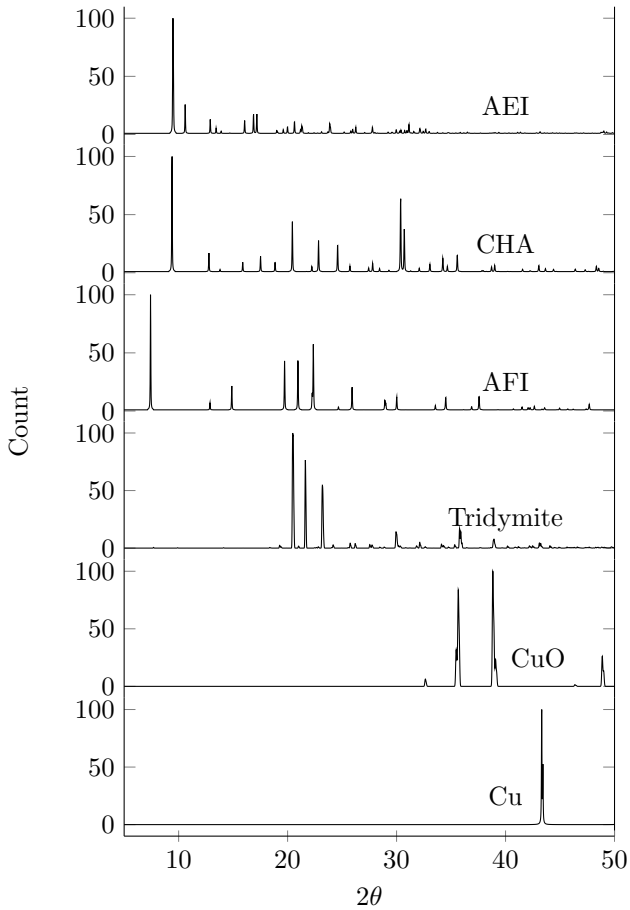

Figure 2.6: XRD patterns of AEI, CHA, AFI, Tenorite (CuO) and metallic copper (Cu).

2.5.2 BET

Brunauer-Emmett-Teller (BET) theory[59] is a commonly applied method for determining the surface area of solids.[60] BET extends Langmuir theory to multilayer adsorption, obtaining the following equation (given in it's linearised form) relating the pressure of adsorptive, p to the monolayer volume of adsorbate, v_m

$$\frac{p}{v \cdot (p^\circ - p)} = \frac{1}{v_m \cdot C} + \frac{(C-1)}{v_m \cdot C}\frac{p}{p^\circ} \tag{2.6}$$

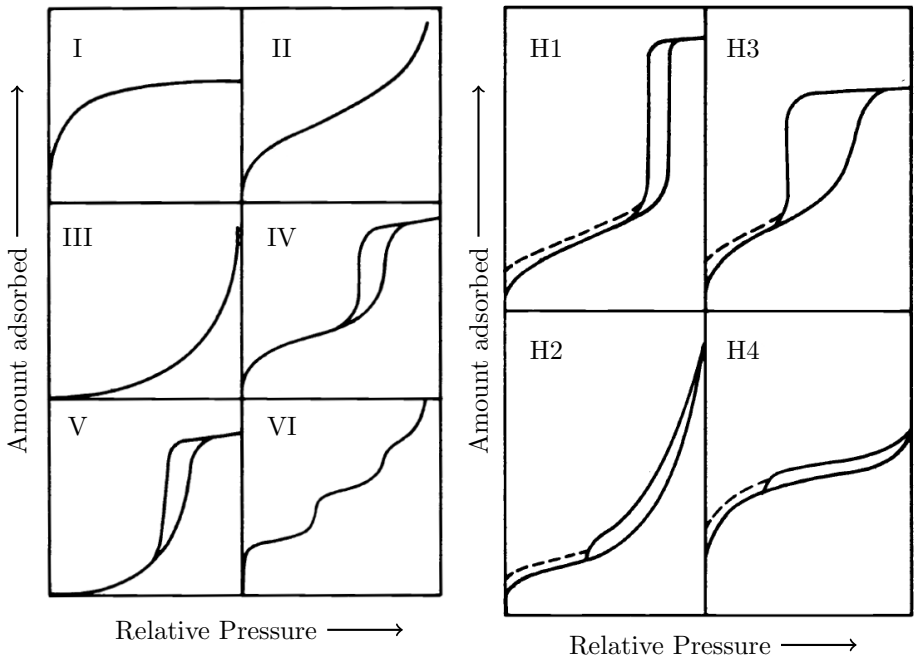

Figure 2.7: Types of physisorption isotherms (left) and types of hysteresis loops (right). Reproduced with permission from Sing[60] (©1985 IUPAC).

where p° is the standard pressure, v is the volume of adsorbed, and C is an empirical measure with a relation to the heat of adsorption.[60] v_m relates to the adsorbent surface area via the known volume of a single adsorbate.

When measuring materials which possess porosity, the adsorbed volume measured differs between adsorption and desorption giving rise to a hysteresis loop[60] (see in particular type IV in Figure 2.7). This is due to capillary condensation due to porosity and so the hysteresis shape can be used to gain some insight into the type of porosity present in the material. Of interest to this work is the fact that hysteresis where there is a relatively constant difference generally comes from agglomerated of platelets or slit-like pores (type H3 or H4 in Figure 2.7), as such morphologies is typically observed for SAPO-18.[1]

t-plot method is a refinement on BET where comparing the isotherm of microporous material with that of a non-porous material. By plotting the adsorption thickness (t) versus quantity adsorbed, the microporous and external surface areas can be obtained. Here external area means all non-microporous area.[60]

In the present work BET analysis is used to obtain the BET surface area, and the *t*-plot method is used to obtain the micropore and external surface areas. All methods are used as implemented in the instrument software.

2.5.3 ICP-MS

Inductively Coupled Plasma Mass Spectroscopy (ICP-MS) is a quantitative element characterization method, in which an analyte solution is aerosolised and then converted into ions via a plasma. Thus produced ions are then characterized via a mass spectrometer.[61]

In the present work ICP-MS is used to obtain the composition of the formed solid samples, with particular interest in the Si and Cu contents.

2.5.4 FT-IR

Infra-red (IR) spectroscopy probes the vibrational mode of functional groups in a material. Only the modes which involve a change in dipole moment are active in IR.[62] Each band or peak in an IR spectrum can be associated with a specific vibrational mode of a functional group.

Of interest to this work is the hydroxy area (3900-3200 cm^{-1}) of the spectrum (Figure 2.8). SAPO-18 possesses two sets of bands in this region;[7] those from surface groups and those from Brønsted acid sites. The surface groups are located as Al–OH: 3794, 3767 cm^{-1}; Si–OH: 3743 cm^{-1}; and P–OH: 3680 cm^{-1}. There are two Brønsted acid sites from the incorporation of Si depending on where the Si–OH–Al bridge is located. Acid groups in the cages give a band at 3628 cm^{-1} while groups in the D6R units give a band at 3606 cm^{-1}. On the back of other metals (Co, Mg, Ni, Zn; see Figure 2.9), copper Brønsted acid sites can be expected to give bands somewhere in the range of 3650–3400 cm^{-1}.[7]

Adsorption of CO onto the Brønsted acid sites in a material causes a negative shift in vibrational frequency (by approximately 270 cm^{-1} for CHA and AEI type materials).[7,63] Non-acidic hydroxyl groups (i.e. surface groups) do not undergo such shifts. The band from free CO ($\sim$2140 cm^{-1})[63,64] shifts depending on the kind of site adsorbed to. Adsorption onto Brønsted acid sites give bands around 2177 cm^{-1} while adsorption onto silanol groups give band at $\sim$2160 cm^{-1}.[63] CO adsorbed to Cu^{+} give a band around 2120 cm^{-1} while adsorption onto Cu^{2+} gives a band around 2150 cm^{-1}.[65,66]

In the present work FTIR is used attempting to assess the location of Si and Cu by probing any Brønsted acid sites formed. Of particular interest is the detection of Brønsted acid sites formed by the incorporation of copper.

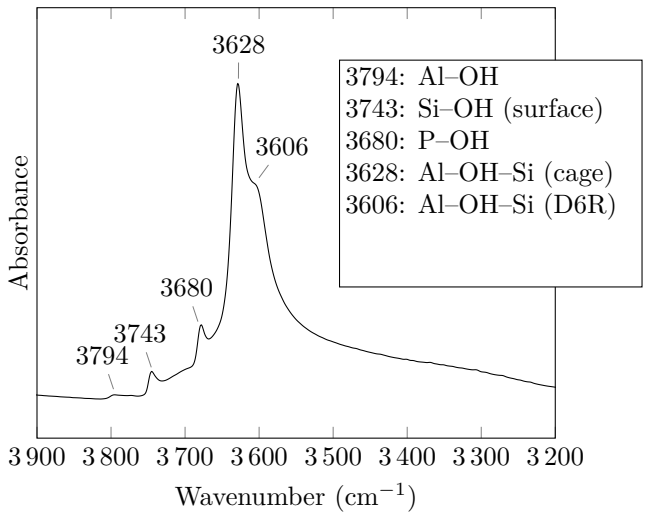

Figure 2.8: The hydroxy area of a FTIR spectra of a representative SAPO-18 material. Assignments according to Chen and Thomas.[7] Spectrum is from sample DIPEA-Ref-8d presented later.

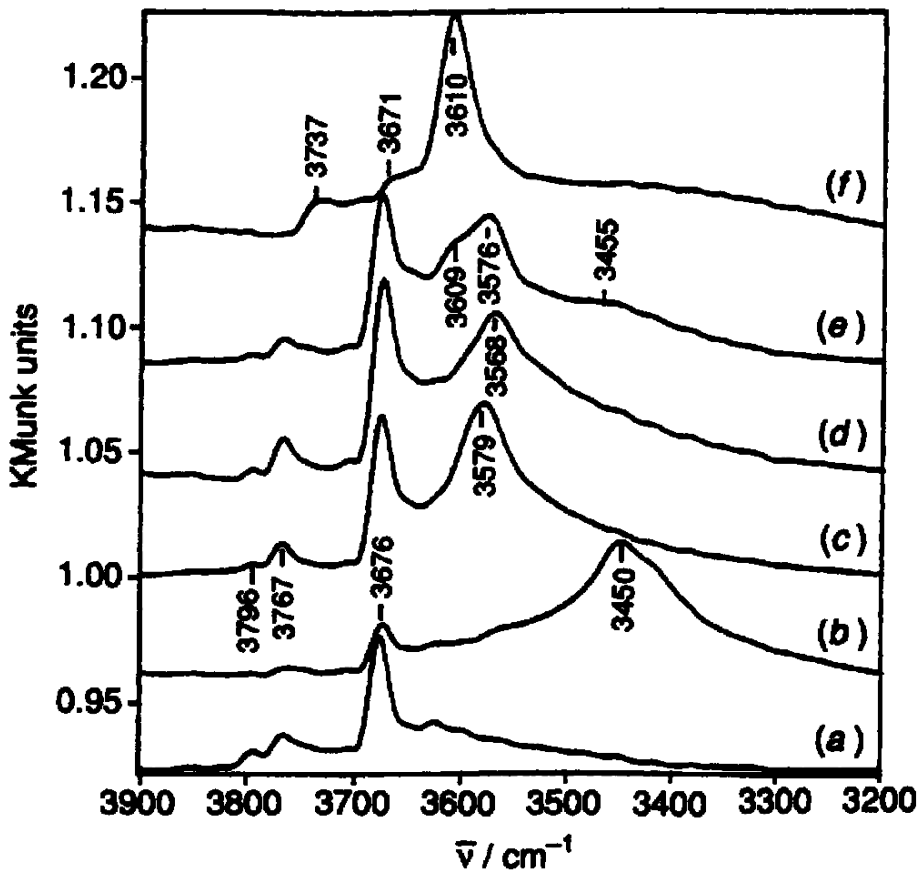

Figure 2.9: The hydroxy area of FTIR spectra of MAPO-18s (M=(a) —, (b) Ni, (c) Zn, (d) Co, (e) Mg). (f) is HZSM-5. Reproduced from Chen and Thomas[7] with permission of Royal Society of Chemistry.

2.6 SCR of NO_x

NO_x gasses, which are notably formed in combustion engines, is a key contributor to acid rain through the formation of nitric acid

$$2\,NO_2 + H_2O \longrightarrow HNO_3 + HNO_2 \tag{2.7}$$

The conventional means to remove NO_x gasses from exhaust is noble metal based three way converter and selective catalytic reduction using ammonia (NH_3-SCR).[67] The former is poor for diesel systems as it is deactivated by SO_2 present in such exhaust and the latter requires a supply of ammonia, which is fine for commercial environments but for private vehicles is prohibitively inconvenient. A proposed alternative is selective catalytic reduction using hydrocarbons (HC-SCR) already present in the exhaust, eliminating the need for an additive.

The general reaction for SCR or NO_x can be described as:[68,69]

$$R + NO + O_2 \longrightarrow N_2 + H_2O + R' \tag{2.8}$$

where R is a reductant; either NH_3 or a hydrocarbon such as propene, and R′ is the resultant oxidative product; either N_2 or CO_2 respectively. The actual reactions occurring are numerous and complicated.[68]

Martínez-Franco et al.[12] reported high conversion of NO (> 80%; 400 ppm NO) over a wide range of temperatures (250-500 °C) for Cu^{2+} ion-exchanged and ion-exchange-like Cu-SAPO-18 using NH_3 as the reductant. For similar Cu-SAPO-18 materials Chen et al.[13] reported conversion above 90% (1000 ppm NO) for 225-525 °C. No reports of HC-SCR on SAPO-18 have been found. However, Cu^{2+} ion-exchanged SAPO-34 has been studied in HC-SCR with some success. Ishihara et al.[70] reported high activity (∼60% conversion; 1000 ppm NO) from 200-600 °C for Cu^{2+} ion-exchanged SAPO-34. Previous in-group work[42,71] obtained similar results on ion-exchanged SAPO-18 using conditions identical to those used herein other than using dry feed. Other work[43] investigating SAPO-34 which contained copper through synthesis (the exact state(s) could not be established), found an activity close to 60% for a range of temperatures which lowered depending on copper content. (The lowest range was 375-425 °C.) All these workers obtained a broad activity curve, generally with a range of temperatures were the conversion was largely constant. However, previous work has also found samples were activity was a maximum at 500 °C and dropping rapidly (Cu^{2+} ion-exchanged SAPO-34).[72]

Herein the activity of samples towards HC-SCR is used as a potential indicator of the form and availability of copper in the samples.

Chapter 3

Experimental

3.1 Synthesis

Materials were synthesised using a hydrothermal method. Samples are divided by the template utilized. Preparation of materials for comparison in SCR of NO_x is given in Section 3.1.3.

In a typical synthesis (using either a 40 or 100 mL autoclave; masses given for the latter), colloidal silica (SiO_2, 40 wt%, 2.4 or 0.5 g, Aldrich), deionized water (H_2O, 100%) and pseudobohemite (AlO(OH), 71.8% or 75%, 7–8 g, provided free of charge by SASOL) were added to orthophosphoric acid (H_3PO_4, 85%, 10 g, Merck). This gel was then aged for 2 h before adding template (either DIPEA ($C_8H_{19}N$, 98%, 12 g, Acros Organics) or TEAOH ($C_8H_{20}NOH$, 40 wt%, ∼40 g, Sigma Aldrich)). Ageing refers to stirring the gel for a set time, while covered to avoid loss of water or other constituents. Between each addition the gel was allowed to homogenize (usually <5 min). Gels were prepared to a molar ratio reported as

$$Al_2O_3 : xH_3PO_4 : ySiO_2 : zTEAOH : wH_2O$$

Prepared gel was in all cases transferred to a 40 or 100 mL teflon lined autoclave for crystallization. Batches were scaled so the autoclave was approximately two-thirds full in each case.

After crystallization (200–150 °C for 4–16 d) samples were washed four times with deionized water before drying overnight at 70 °C.

Samples were calcined using a ramp of 1 °C min^{-1} and held for 6 h at 550 °C.

Sample names take the form Template-Parameters@T, where Template is DIPEA or TEAOH and T is the crystallization temperature in °C. Parameters give the value of key synthesis parameters for the specific sample. For example samples where the water content were varied are named with -wN were N is the

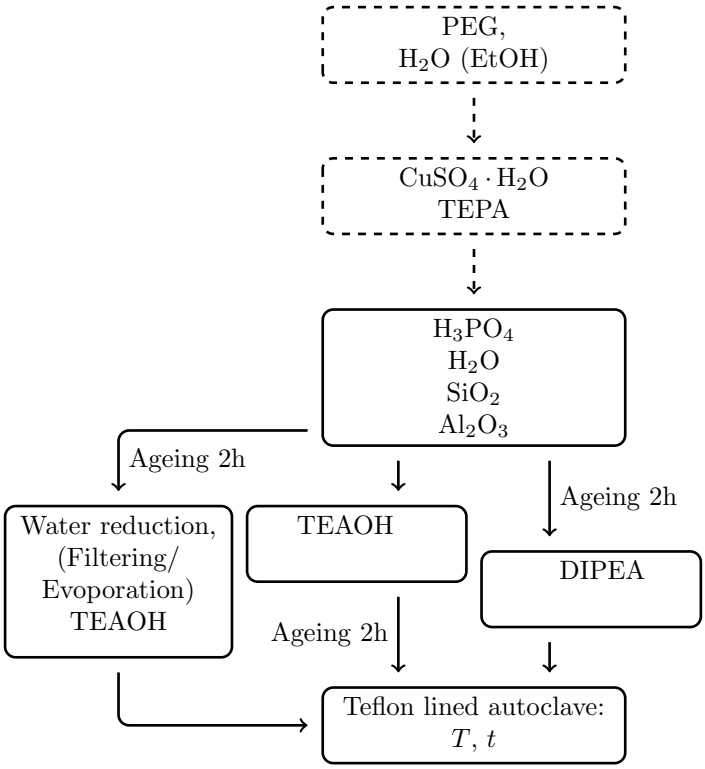

Figure 3.1: General synthesis order. Dashed lines indicate variant additions.

gel water ratio. Similarly -4d is used for sample with a crystallization time of 4 days. If no letter is given Parameters are given as -x-y were x and y are the H_3PO_4 and template gel ratios respectively. The sample names are given for each synthesis.

3.1.1 DIPEA based synthesises

Reference SAPO-18 material was synthesised using DIPEA based on the ratio from Martínez-Franco et al.[12] Crystallization temperature and time were 180 °C and 8 d respectively. Additional samples were made by halving (4 d) and doubling (16 d) the crystallization time. The sample gel ratios are given in Table 3.1.

Table 3.1: Gel ratios of reference samples synthesised using DIPEA. All samples crystallized at 180 °C.

Sample	H_3PO_4	SiO_2	DIPEA	H_2O	t_{crys} [d]
DIPEA-Ref-4d	1.71	0.42	1.82	38.27	4
DIPEA-Ref-8d	1.73	0.28	1.73	37.55	8
DIPEA-Ref-16d	1.70	0.30	1.77	37.95	16

Samples attempting to include copper in a DIPEA synthesis were made by dissolving $CuSO_4 \cdot H_2O$ (1.4 g, Riedd de Haën) in water before adding TEPA ($C_8H_{23}N_5$, 1.1 g, Aldrich). To this solution other reagents were added following the procedure described above. Temperature was varied based on results from the sample crystallized at 180 °C, see Section 4.2. For completeness, a sample was synthesised at 150 °C without TEPA present. Gel ratios of these samples are given in Table 3.2.

Use of PEG to obtain hierarchical SAPO-18 was based on Nazari et al.[8] Synthesis using PEG necessitated additional solvent to able to disperse the PEG. Samples were synthesised by dispersing PEG (∼8 g, Aldrich) in H_2O or EtOH (C_2H_5OH, 100%, VWR Chemicals), before proceeding with synthesis as normal. Samples are named DIPEA-PEG and DIPEA-PEG-EtOH for samples with added water and EtOH respectively. Samples were synthesised using both PEG and TEPA by dispersing PEG in solvent before adding $CuSO_4 \cdot H_2O$ then TEPA and continuing synthesis as normal. These samples are numbered by order of synthesis. Gel ratios of such samples are given in Table 3.3.

Table 3.2: Gel ratios of samples synthesised using DIPEA, $CuSO_4 \cdot H_2O$, and TEPA.

Sample	H_3PO_4	SiO_2	CuO	TEPA	DIPEA	H_2O	T, t [°C, d]
DIPEA-TEPA-Cu-180	1.81	0.30	0.166	0.11	1.76	38.15	180, 8
DIPEA-TEPA-Cu-150	1.82	0.23	0.135	0.09	1.68	33.98	150, 8
DIPEA-TEPA-Cu-16d	1.70	0.38	0.145	0.10	1.52	35.70	150, 16
DIPEA-Cu-150	1.73	0.33	0.153	—	1.78	30.83	150, 8

Table 3.3: Gel ratios of samples synthesised using DIPEA, TEPA and PEG.

Sample	H_3PO_4	SiO_2	CuO	TEPA	DIPEA	H_2O	PEG	EtOH
DIPEA-PEG	2.00	0.40	—	—	1.88	74.46	0.065	—
DIPEA-PEG-EtOH	1.79	0.36	—	—	1.88	36.20	0.059	11.51
DIPEA-PEG-TEPA-1	1.88	0.96	0.188	0.18	1.50	44.24	0.061	11.34
DIPEA-PEG-TEPA-2	2.21	0.44	0.169	0.34	1.62	36.36	0.062	11.92
DIPEA-PEG-TEPA-3	3.36	0.46	0.206	0.43	2.38	69.86	0.075	—

3.1.2 TEAOH based synthesises

Initial synthesis of SAPO-18 using TEAOH was based on the ratio of Turrina et al.[47] Initial sample corresponds to the (1.2, 0.5) sample in the following set. Additional samples were made varying the H_3PO_4 and TEAOH content (0.7, 1.2, 1.7 and 0.3, 0.5, 0.8). Ratios were varied greatly to attempt find a gel ratio which can produce SAPO-18. Gel ratios are given in Table 3.4.

Table 3.4: Gel ratios of initial samples synthesised using TEAOH.

Sample	H_3PO_4	SiO_2	TEAOH	H_2O
TEAOH-0.7-0.7	0.68	0.394	0.72	47.37
TEAOH-0.7-0.6	0.73	0.417	0.60	50.54
TEAOH-0.7-0.3	0.70	0.403	0.30	46.75
TEAOH-1.2-0.8	1.21	0.385	0.82	52.74
TEAOH-1.2-0.5	1.26	0.313	0.53	50.42
TEAOH-1.2-0.3	1.24	0.405	0.30	48.33
TEAOH-1.7-0.8	1.68	0.431	0.79	52.87
TEAOH-1.7-0.5	1.79	0.399	0.50	49.92
TEAOH-1.7-0.3	1.89	0.434	0.32	51.46

A second set of samples were synthesised based on the ratios of Wendelbo et al.[1] The initial gels made formed a solid upon addition of pseudobohemite. These synthesises had to be terminated, as the formed solids were not dispersible in the TEAOH solution. To circumvent this, the following variations were made to the synthesis. For these samples the gel ratio was

$$Al_2O_3 : 2.00H_3PO_4 : .092SiO_2 : 2.00\text{TEAOH} : wH_2O$$

where w is the water content. The variations and water content are summarized in Table 3.5. First, water content was increased ($w = 65$) for samples TEAOH-w65-@200 and TEAOH-w65-@150. Samples were also synthesised where template was added rapidly after pseudobohemite and then aged (TEAOH-w40-@200 and TEAOH-w40-@150; $w = 40$).

To investigate the effect of ageing for synthesis at 150 °C, additional water was included at the mixing stage and removed after ageing ($w = 41$) by heating and allowing water to evaporate (TEAOH-evaporation). Removal of water was also attempted using filtration. Gel containing additional water was transferred to a Büchner-funnel with 413 filter paper (5-13 µm particle retention, VWR Chemicals). Water suction was applied until no more liquid could be seen coming out ($w = 43$). The filter cake thus obtained was used as the gel for the remaining procedure (TEAOH-filtration). Water content varied between samples as more water could not be removed from the gels. A sample (TEAOH-Cu-filtration) was

Table 3.5: Table of samples synthesised with different variations pertaining to water content of the gel. What was added prior to ageing and method of removal is given along with obtained H_2O content. T gives the crystallization temperature.

Sample	Added	Removed	H_2O	T [°C]
TEAOH-w65-@200	H_2O	—	65	200
TEAOH-w65-@150	H_2O	—	65	150
TEAOH-w40-@200	TEAOH	—	40	200
TEAOH-w40-@150	TEAOH	—	40	150
TEAOH-evaporation	H_2O	Evaporation	41	150
TEAOH-filtration	H_2O	Filtration	43	150
TEAOH-Cu-filtration	H_2O, CuO	Filtration	51	150
TEAOH-HAc@200	HAc	—	40	200
TEAOH-HAc@150	HAc	—	40	150
TEAOH-TMAOH	TMAOH, TEAOH	—	40	150
TEAOH-TPAOH	TPAOH, TEAOH	—	40	150

synthesised including additional water and CuO (0.098 g, VWR Chemicals), and water was attempted removed using filtration under water suction ($w = 51$).

As a preliminary test to use tetraethylammonium acetate (TEAAc) as the template source, samples were synthesised adding equimolar acetic acid (HAc, $C_2H_4O_2$, ∼7 g, Merck) to template. Sample gel ratios were

$$Al_2O_3 : 2H_3PO_4 : 0.06SiO_2 : 2TEAOH : 39.5H_2O : 2HAc$$

Addition of HAc allowed for aging of the gel. Samples were crystallized at 200 °C (TEAOH-HAc@200) and 150 °C (TEAOH-HAc@150) for 8 d. Use of TEAAc was not investigated.

The effect of replacing a small amount of TEAOH with related templates tetrametylammonium hydroxide (TMAOH, $C_4H_{12}NOH$, 25%, 1.2 g, Aldrich) and tetrapropylammonium hydroxide (TPAOH, $C_{12}H_{28}NOH$, 40 wt% 1.7 g,) was investigated. Sample were synthesized using

$$Al_2O_3 : 2H_3PO_4 : 0.08SiO_2 : 1.75TEAOH : 38H_2O : 0.05R$$

where R is either TMAOH or TPAOH (samples TEAOH-TMAOH and TEAOH-TPAOH). Samples were crystallized at 150 °C for 8 d.

Based on the result of these variations, template was added prior to ageing for the following samples investigating the effect of varying the H_3PO_4 and TEAOH content. Gel ratios for these samples were

$$Al_2O_3 : xH_3PO_4 : 0.07SiO_2 : yTEAOH : 40H_2O$$

Table 3.6: Gel ratios of samples synthesised using varying H_3PO_4 and TEAOH content with or without copper and at 150 or 200 °C. All samples were crystallized for 8 d.

Sample	H_3PO_4	TEAOH	CuO	T [°C]
TEAOH-2.2-2.2@200	2.2	2.2	—	200
TEAOH-2.0-2.2@200	2.0	2.2	—	200
TEAOH-2.2-2.0@200	2.2	2.0	—	200
TEAOH-2.0-2.0@200	2.0	2.0	—	200
TEAOH-1.8-2.0@200	1.8	2.0	—	200
TEAOH-2.0-1.8@200	2.0	1.8	—	200
TEAOH-1.8-1.8@200	1.8	1.8	—	200
TEAOH-1.6-1.8@200	1.8	1.6	—	200
TEAOH-1.6-1.6@200	1.6	1.6	—	200
TEAOH-2.2-2.0@150	2.2	2.0	—	150
TEAOH-2.0-2.0@150	2.0	2.0	—	150
TEAOH-2.2-1.8@150	2.2	1.8	—	150
TEAOH-2.0-1.8@150	2.0	1.8	—	150
TEAOH-Cu-2.2-2.0	2.2	2.0	0.053	150
TEAOH-Cu-2.2-1.8	2.2	1.8	0.051	150
TEAOH-Cu-2.0-1.8	2.0	1.8	0.054	150
TEAOH-Cu-1.6-1.8	1.6	1.8	0.053	150
TEAOH-Cu-1.85-1.65	1.85	1.65	0.064	150
TEAOH-Cu-1.6-1.7	1.6	1.7	0.050	150
TEAOH-Cu-2.0-1.6	2.0	1.6	0.050	150

where x and y were varied between 1.6 and 2.2 and crystallized at 200 °C or 150 °C in combinations given in Table 3.6. Samples were also synthesized including copper using the gel ratio

$$Al_2O_3 : xH_3PO_4 : 0.07SiO_2 : 0.05CuO : y\text{TEAOH} : 38H_2O$$

with combinations of x and y given in Table 3.6.

3.1.3 Post-synthesis Modification

The following samples were prepared to be used as catalysts in SCR of NO_x for comparison against other samples. Ion-exchange samples were prepared by a two step method. Calcined sample was exchanged twice in a 0.10 M NH_4NO_3 solution and twice in a 0.033 M $CuSO_4$ solution, with washing and drying overnight between each step. Samples were again calcined after ion-exchange using a ramp of 1 °C min^{-1} and held for 6 h at 550 °C. DIPEA-Ref-8d and TEAOH-2.0-1.8@200

were exchanged this way and such exchanged samples are annotated with a -IE suffix; DIPEA-Ref-8d-IE and TEAOH-2.0-1.8@200-IE.

Sample TEAOH-2.0-1.8@200-mix-CuO was prepared by mechanically mixing 126 mg of sample TEAOH-2.0-1.8@200 (calcined) with 7.8 mg CuO.

3.2 Characterization

3.2.1 XRD

XRD analysis was carried out using a Bruker D8 A25 DaVinci X-ray Diffractometer using CuKα radiation and a LynxEye^{TM} SuperSpeed Detector. Data was collected from 5-60° with a step size of 0.0134° over 15 min with a variable divergence slit such that a constant 6mm of sample is illuminated.

Stacking Fault Rate (SFR) was determined by simple numerical comparison with the calculated patterns.[54] XRD pattern of calcined sample was background corrected using the method of Gan et al.[73] using a 18-th order polynomial. Measurements between $2\theta = 10$ and 35 was used for these calculations to prevent the 9.5 peak from dominating, and patterns were normalized to have the same maximum height in the selected region. SFR was calculated as the pattern with the lowest mean square error between measured and calculated error. Only growth type faults were utilized. This method estimated SFR to the nearest 0.1 except for values over 0.9 where it found to the nearest 0.02 (values under 0.1 are not relevant for this work). There is little variance for SFR around 0.5, and so this low resolution is acceptable. For this work an SFR of 0.8 or greater has been considered to be AEI.

3.2.2 BET

BET characterization was carried out using a Micromeritics Tristar 3000 Surface Area and Porosity Analyzer. ∼0.2 g sample was degassed in a Micromeritics VacPrep061 at 250 °C overnight to remove adsorbed species directly prior to analysis. Sorption measurements were carried out using N_2 and at 77 K. BET surface area as well as micropore and external surface from the t-plot method was calculated by the instrument software. Linearity of plots were confirmed visually.

3.2.3 ICP-MS

ICP-MS was carried out by Syverin Lierhagen (IKJ) on a High Resolution Inductively coupled plasma Element 2 (Thermo Electronics) coupled to a mass spectrometer. Analysis solutions were prepared by decomposing 15–45 mg solid sample in 1.5 mL conc. nitric acid (HNO_3, 65%) and 0.5 mL conc. hydroflouric

acid (HF) for at least 30 min before diluting to 205–240 mL. 16 mL Teflon sample tubes were washed thrice with diluted solution before being filled and delivered for analysis.

3.2.4 FT-IR

FT-IR was performed using a Bruker VERTEX 80 FTIR spectrometer and a liquid nitrogen cooled HgCdTe detector (LN-MCT). Aperture opening was 2 mm and the scan frequency $4\,\mathrm{cm}^{-1}$. Samples were placed in a glass cell with KBr windows and which could be attached to a vacuum line. Samples were pressed into self supporting wafers (11.9 mg) using an hydraulic press and a pressure of 5 tons. Prior to measurements samples where heated to 500 °C using a ramp of $5\,°\mathrm{C\,min}^{-1}$ and held for 1 h under vacuum (approx. 1×10^{-7} bar) to remove any adsorbed species (in particular H_2O). After heating sample was allowed to cool to room temperature while disconnected from the vacuum line. Background measurements were taken, before the cell was cooled with liquid nitrogen. While cooled, the cell was exposed to a CO pressure of approximately 1 mbar which was then evacuated incrementally with spectrum taken at each step.

3.3 SCR of NOx

SCR of NO_x was performed in a tubular plug reactor using the setup shown in Figure 3.2. Catalyst sample was pressed into wafers and gently crushed to obtain particles between 212 and 425 µm. Such prepared sample (approx 110 mg) was secured in the middle of the reactor tube using quartz-wool plugs. Catalyst was heated overnight to 500 °C under a flow of Ar ($10\,\mathrm{mL\,min}^{-1}$), before activating in 2% O_2 for 1 h. Reaction was run using a flow of 2000 ppm NO, 1200 ppm C_3H_6, 2% O_2 and Ar (total flow $140\,\mathrm{mL\,min}^{-1}$). One Ar line was bubbled through water heated to 50 °C in order to obtain a wet feed. Concentration of NO was measured using a Eco Physics CLD 60 Chemiluminescence NO/NO_x Analyser. A condenser was attached ahead of the detector prevent water from damaging the instrument. Temperature was decreased in 25 °C steps down to 275 °C and held at each temperature for 20 min. At temperatures where bypass was measured the hold time was extended to 40 min.

To assess the concentration behaviour of the system, two runs were performed without a catalyst present and where bypass measurements were taken at every step. These showed that NO_x concentration fell as a exponential function:

$$y = c_0 + c_1 \exp(-c_2 \cdot t) \tag{3.1}$$

where y is NO_x concentration, c_0, c_1, c_2 are fitting parameters, and t is time elapsed. The two runs showed different parameters c_0, c_1, c_2. Therefore for each

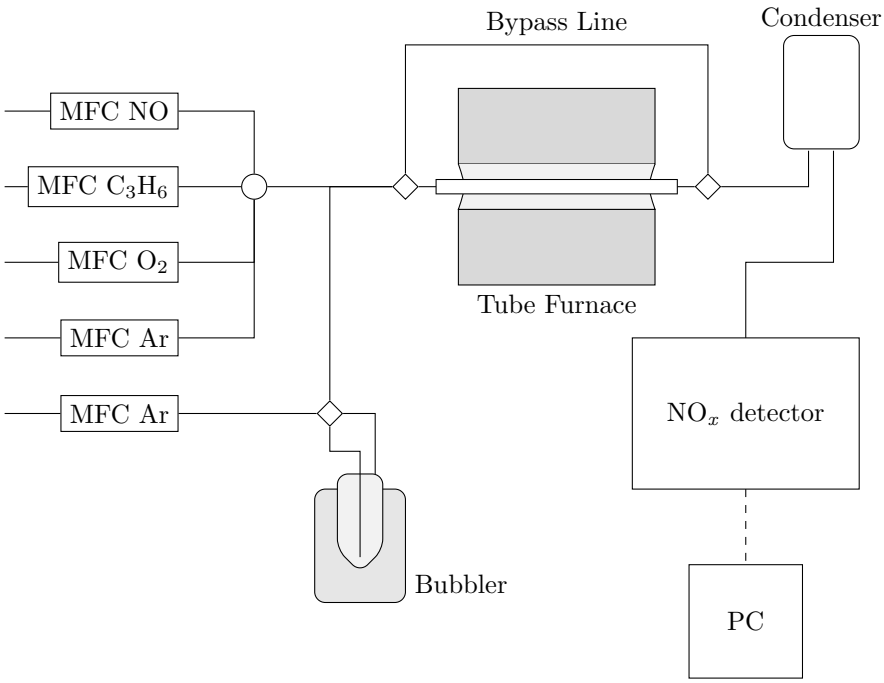

Figure 3.2: Schematic of system used for catalysis. MFC = Mass Flow Controller.

run, bypass was measured at the beginning, the end and while at 400 °C. An exponential function of the form of Equation 3.1 was fitted to these measurements and used as the feed concentration. Conversion was calculated as a function of time by

$$X(t) = \frac{y(t) - y_{\mathrm{NOx}}(t)}{y(t)} \tag{3.2}$$

where X is the conversion, y is the feed concentration and y_{NOx} is the measured concentration. For each temperature, the average conversion over the last minute was used as the conversion at that temperature.

Chapter 4

Results

4.1 Observations

As copper containing materials will have a colour which depends the coordination and ligands of copper, valuable information can be obtained from simply looking at the samples. All samples made without copper were white (see Figure 4.1 a).

With the initial sample made using DIPEA and TEPA (DIPEA-TEPA-Cu-180) the liner contained both a brown sludge and blue crystals. The brown sludge was assumed to consist of metallic copper and decomposed DIPEA and was discarded. The blue crystals were kept as the sample. Sample crystallized at lower temperature (DIPEA-TEPA-Cu-150) was also blue (Figure 4.1 b) which turned grey upon calcination (Figure 4.1 c), indicating formation of copper oxide. Sample made without TEPA (DIPEA-Cu-150) was a light pink (Figure 4.1 d), indicating copper present as metal.

Samples synthesised using PEG and TEPA were blue prior to, and turned black upon calcination (Figure 4.1 e-h for DIPEA-PEG-TEPA-2 as prepared and calcined and DIPEA-PEG-TEPA-3 as prepared and calcined respectively.) The black colour indicates formation of copper oxide. Blue colour is consistent with H_2O coordinated to Cu^{2+}

For all samples including CuO using TEAOH except TEAOH-Cu-2.0-1.6, reddish-brown particles were observed along with pale blue crystals. These particles were not visible after drying. Their presence indicates some copper was reduced to metal. Upon calcination these samples went from pale blue to pale green (Figure 4.1 i-j for TEAOH-Cu-2.0-1.8 and k-l for TEAOH-Cu-2.0-1.6). pH of gel prior to and that of supernatant solution after crystallization for select samples is given in Table 4.1. pH of gels was generally slightly lower for samples with more H_3PO_4 relative to TEAOH. For TEAOH-Cu-2.0-1.6 which has the

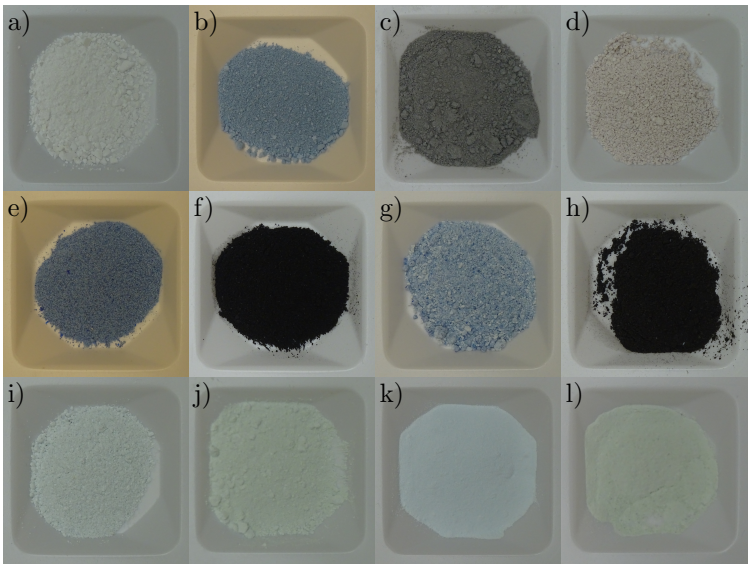

Figure 4.1: Pictures of select samples; a) DIPEA-Ref-8d, b) DIPEA-TEPA-Cu-16d, c) DIPEA-TEPA-Cu-16d calcined, d) DIPEA-Cu-150, e) DIPEA-PEG-TEPA-2, f) DIPEA-PEG-TEPA-2 calcined, g) DIPEA-PEG-TEPA-3, h) DIPEA-PEG-TEPA-3 calcined, i) TEAOH-Cu-2.0-1.8, j) TEAOH-Cu-2.0-1.8 calcined, k) TEAOH-Cu-2.0-1.6, l) TEAOH-Cu-2.0-1.6 calcined.

greatest such ratio the supernatant solution had a lowered pH (9 as opposed to 10).

For the sample including CuO and attempting to remove water by filtration (TEAOH-Cu-filtration), the filtrate was pale blue, and had a pH ≈ 2 indicating that both copper and phosphoric acid are lost during this synthesis step. Amounts lost were not investigated.

Ion-exchanged samples (DIPEA-Ref-8d-IE and TEAOH-2.0-1.8@200-IE) were pale blue both before and after calcination.

Table 4.1: pH of gel prior to and supernatant solutions (SNS) after crystallization for select samples. For copper containing samples, whether metallic copper was observed upon opening the autoclave is given.

Sample	Gel	SNS	Met. Cu observed
TEAOH-2.2-2.0@150	6–7	10	—
TEAOH-2.2-1.8@150	5–6	10	—
TEAOH-Cu-2.2-1.8	6	10	Yes
TEAOH-Cu-2.0-1.8	—	10	Yes
TEAOH-Cu-2.0-1.6	5–6	9	No

4.2 XRD

In order to obtain the formed phase(s) of samples, and in particular verify the formation of SAPO-18 (AEI phase), XRD has been employed. Samples are split based on the template used.

4.2.1 DIPEA based samples

Result of all samples synthesised using DIPEA are summarized in Table 4.2. XRD patters of plain SAPO-18 materials synthesised with DIPEA with varying crystallization time are given in Figure 4.2. All samples show distinct AEI patterns, however both 4d and 16d show a sharp peak at 11.8 (red mark). As such only the 8d sample was calcined, pattern given in Figure 4.3. The origin of this extra peak has not been determined.

The XRD pattern of the blue crystals of sample DIPEA-TEPA-Cu-180 is shown in Figure 4.4 (topmost) and show it to be a mix of AFI, AEI, and metallic copper. Samples synthesised at lower temperature (DIPEA-TEPA-Cu-150, DIPEA-TEPA-Cu-16d) does not show an AFI phase (patterns also in Figure 4.4), but appears as a mix of AEI and metallic copper. There does not appear to be any effect of increased crystallization time between the two samples. Upon calcination sample DIPEA-TEPA-Cu-16d transforms to a mix of AEI and tenorite (CuO). Sample synthesised using DIPEA and copper but not TEPA (DIPEA-Cu-150) shows a mix of AEI and metallic copper.

XRD pattern for samples synthesised with PEG and additional H_2O (DIPEA-PEG) or EtOH (DIPEA-PEG-EtOH) are shown in Figure 4.5. The sample with added water shows distinct AEI, whereas sample with added EtOH is also AEI, but has broader, less distinct peaks indicating more disorder in the material. Samples synthesised with PEG and TEPA-Cu^{2+} gave different phases which can't be assigned as AEI (Figure 4.6). DIPEA-PEG-TEPA-1 appears to be mixture of pseudobohemite, AEI, AFR (green stars), as well as metallic copper (blue

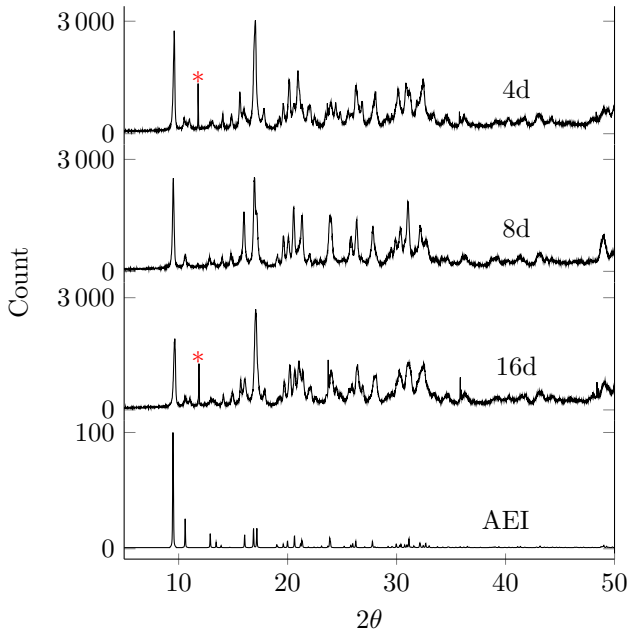

Figure 4.2: XRD patterns for as prepared conventional SAPO-18 samples synthesised with different crystallization times at 180°C (samples DIPEA-Ref-nd). Red stars mark impurity peaks, see text.

star). For both DIPEA-PEG-TEPA-2 and DIPEA-PEG-TEPA-3 the as prepared samples show strong (approx. 3000 count) peaks at $2\theta = 9.6$ which is close to the AEI peak ($2\theta = 9.5$) however neither has other notable peaks corresponding with AEI. Upon calcination both transform to be largely amorphous with minor tridymite and tenorite (CuO) phases.

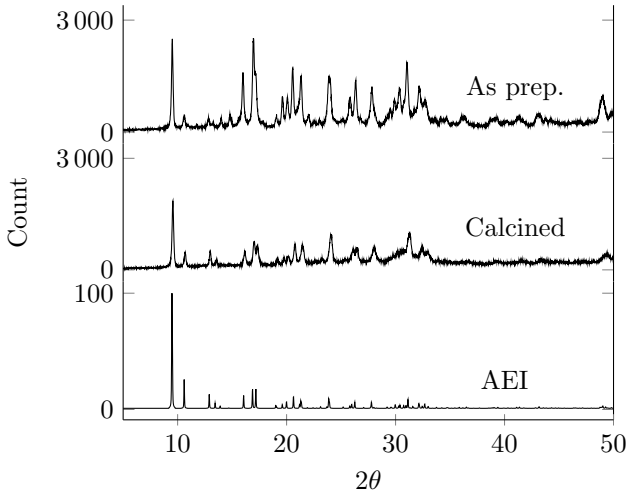

Figure 4.3: XRD patterns for as prepared and calcined at 550°C for 6h DIPEA-Ref-8d.

Table 4.2: Formed phase as determined by XRD for samples synthesised using DIPEA. Samples which obtained phase pure AEI phase are highlighted in green.

			Phase obtained	
Sample	Defining variation	T [°C]	As prepared	Calcined
DIPEA-Ref-4d	Cryst. $t = 4\,\mathrm{d}$	180	AEI + *unknown*[a]	—
DIPEA-Ref-8d	Cryst. $t = 8\,\mathrm{d}$	180	AEI	AEI
DIPEA-Ref-16d	Cryst. $t = 16\,\mathrm{d}$	180	AEI + *unknown*[a]	—
DIPEA-TEPA-Cu-180	TEPA+Cu^{2+}	180	AEI + AFI + Cu metall	—
DIPEA-TEPA-Cu-150	TEPA+Cu^{2+}	150	AEI + Cu metall	—
DIPEA-TEPA-Cu-16d	TEPA+Cu^{2+}, 16 d	150	AEI + Cu metall	AEI + CuO
DIPEA-Cu-150	Cu^{2+}	150	AEI + Cu metall	—
DIPEA-PEG	PEG+H_2O	150	AEI	AEI
DIPEA-PEG-EtOH	PEG+EtOH	150	AEI	AEI
DIPEA-TEPA-Cu-180	PEG+TEPA+Cu+EtOH	150	AEI + *others*[b]	—
DIPEA-TEPA-Cu-150	PEG+TEPA+Cu+EtOH	150	*unknown*[c]	CuO + dense[d]
DIPEA-Cu-150	PEG+TEPA+Cu+H_2O	150	*unknown*[c]	CuO + dense[d]

[a] Sharp peak at $2\theta = 11.8^\circ$. Nature of this phase is not determined.
[b] AFR and pseodobohemite.
[c] Only the $2\theta = 9.6^\circ$ visible. Nature of this phase is not determined.
[d] Tridymite

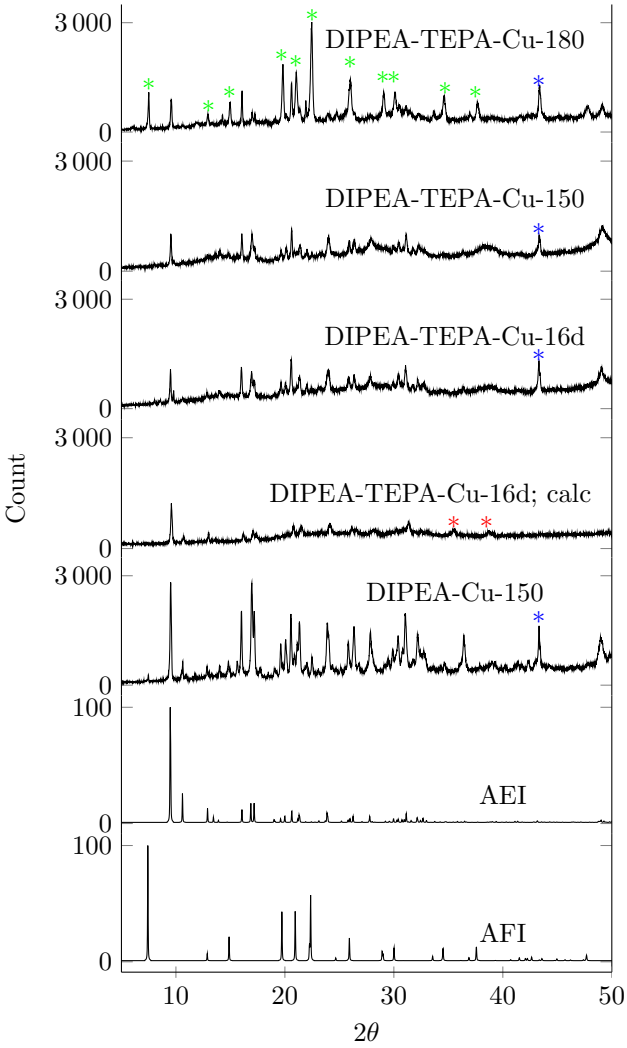

Figure 4.4: XRD patterns for as prepared samples attempting to use TEPA to incorporate copper into conventional SAPO-18. "calc" refers to calcination at 550°C for 6h. Green stars mark AFI peaks, blue stars mark metallic copper peaks, and red stars mark tenorite (CuO) peaks.

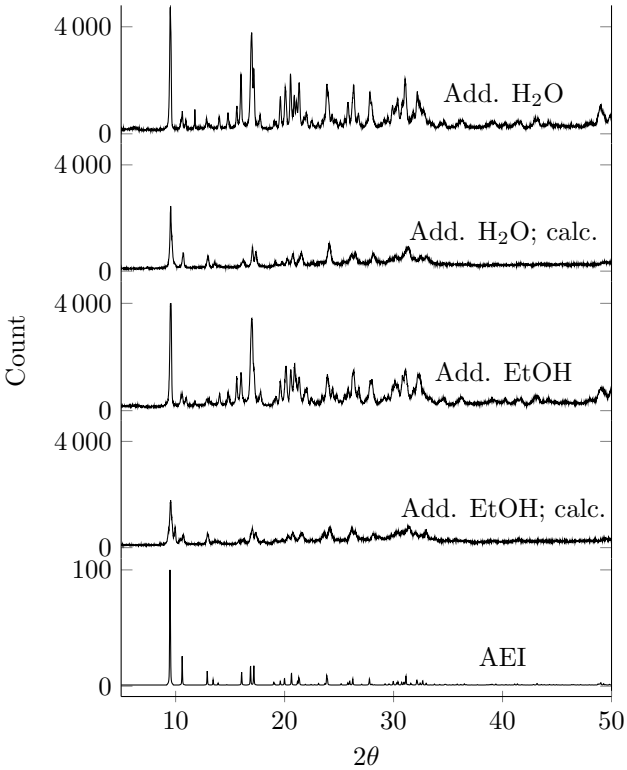

Figure 4.5: XRD patterns for as prepared and calcined samples using PEG as meso-directing agent. "calc." refers to calcination at 550°C for 6h.

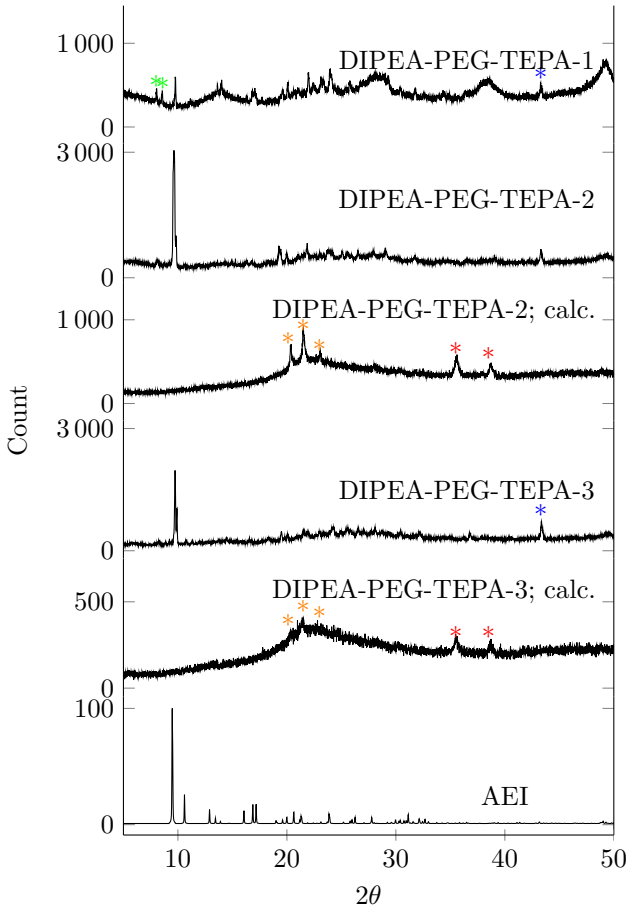

Figure 4.6: XRD patterns for as prepared samples using PEG and TEPA methods. Green stars mark the primary peaks of AFR, blue stars mark metallic copper peaks, orange stars mark tridymite peaks, and red stars mark tenorite (CuO) peaks.

4.2.2 TEAOH based samples

Map of the phases formed when varying H_3PO_4 (0.7, 1.2, 1.7) and TEAOH (0.3, 0.5, 0.8) content is shown in Figure 4.7. XRD patterns are given in appendix (Figures A.1–A.3). Bands can be observed which give no crystalline phase, SAPO-34, SAPO-5, and dense phase tridymite. These bands follow approximately constant TEAOH/H_3PO_4 ratios. As no SAPO-18 formation was observed among these samples, no further synthesis was done among this set.

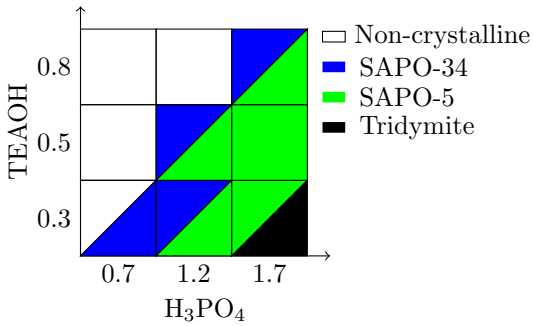

Figure 4.7: Map of formed phases under different H_3PO_4/Al_2O_3 and TEAOH/Al_2O_3 molar ratios.

Phase formed for samples with variations investigated to obtain a synthesis pathway based on the ratio of Wendelbo et al.[1] is summarized in Table 4.3. Samples with increased water content and crystallized at 200 °C (TEAOH-w65-@200) shows a CHA phase (Figure 4.8). However sample crystallized at a lower temperature (TEAOH-w65-@150) does not have any appreciable crystalline phase (Figure 4.8). Similarly for samples where TEAOH was added prior to ageing the low temperature sample (TEAOH-w40-@150) show no crystalline phase, however the high temperature sample (TEAOH-w40-@200) shows a phase which is very close to AEI. However SFR was estimated to be 0.4, which is mostly due to the splitting of the 10.6 peak. It is not clear whether this means formation of an AEI/CHA intergrowth or there is some other, unknown fault.

XRD pattern of samples aged by the use of evaporation (TEAOH-evaporation) and filtration (TEAOH-filtration and TEAOH-Cu-filtration) is given in Figure 4.9. TEAOH-evaporation shows a AEI like pattern with SFR calculated to be 0.92. TEAOH-filtration and TEAOH-Cu-filtration show patterns close to CHA structure, SFR determination has not been performed.

Table 4.3: Phase formed for samples synthesised using TEAOH with various modifications to circumvent the low water content of the gels. What was added and method used to remove water is given. T is the crystallization temperature. All samples were crystallized for 8 d. Samples which successfully gave AEI are highlighted.

				Phase Formed	
Sample	Added	Removed	T [°C]	As prep	Calcined
TEAOH-w65-@200	H_2O	—	200	CHA	CHA
TEAOH-w65-@150	H_2O	—	150	none	—
TEAOH-w40-@200	TEAOH	—	200	AEI	AEI
TEAOH-w40-@150	TEAOH	—	150	none	—
TEAOH-evaporation	H_2O	Evaporation	150	AEI	AEI
TEAOH-filtration	H_2O	Filtration	150	CHA	—
TEAOH-Cu-filtration	H_2O, CuO	Filtration	150	CHA	—
TEAOH-HAc@200	HAc	—	200	AEI + AFI	—
TEAOH-HAc@150	HAc	—	150	AEI + AFI	—
TEAOH-TMAOH	TMAOH, TEAOH	—	150	∼AEI[a]	∼AEI[a]
TEAOH-TPAOH	TPAOH, TEAOH	—	150	∼AEI[a]	∼AEI[a]

[a]The obtained phase is similar to AEI, but not sufficiently well defined to be labelled such.

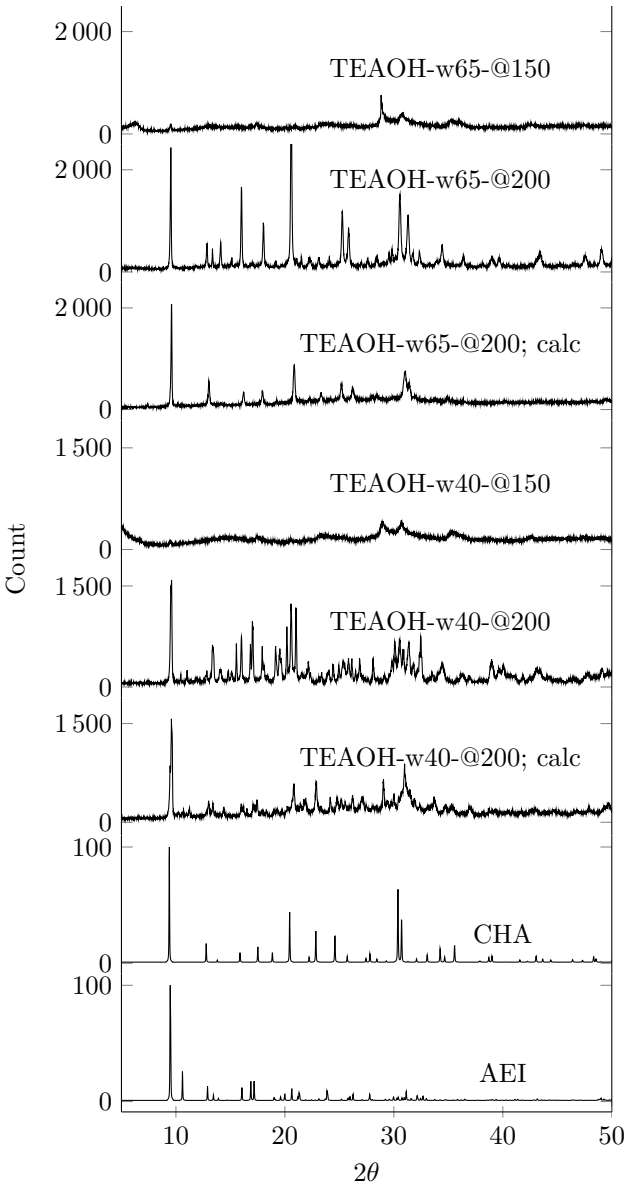

Figure 4.8: XRD patterns of samples synthesised based on the ratio of Wendelbo et al.[1], see text. "calc." refers to calcination at 550°C for 6h.

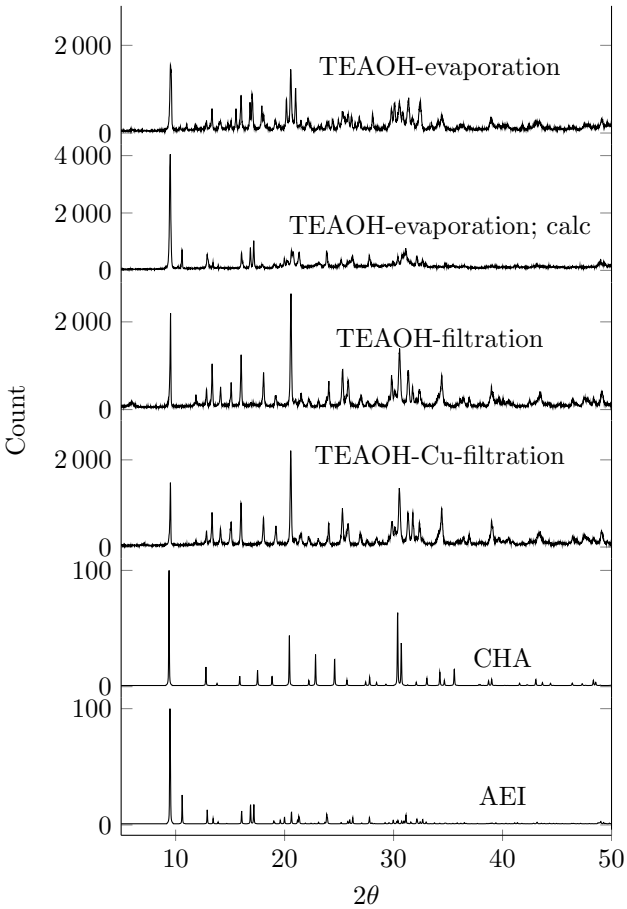

Figure 4.9: XRD patterns of samples synthesized using evaporation or filtration to reduce the water content after aging. "calc" refers to calcination at 550°C for 6h.

Samples synthesised with HAc added to gel (TEAOH-HAc@200 and TEAOH-HAc@150) both show a clear AFI phase in addition to a phase that is either AEI or CHA (Figure A.4). The high temperature sample shows more AFI relative to the other phase than the low temperature sample.

XRD patterns of samples synthesised with some (2.5 molar%) TEAOH replaced by either TMAOH or TPAOH are given in Figure 4.10. Sample TEAOH-2.0-1.8@150 is given as a comparison with pure TEAOH. Both TEAOH-TMAOH and TEAOH-TPAOH show low-crystalline AEI-like patterns which is lowered upon calcination. SFR was not determined.

XRD patterns of calcined samples synthesised varying H_3PO_4 and TEAOH ratios between 1.6 and 2.2 are given in appendix and split by crystallization temperature between Figures A.5 and A.6 (200 °C), Figure A.7 (150 °C), and Figure A.8 (Copper containing samples; 150 °C). The key results therefrom are given in Table 4.4. There is little to no clear pattern among 200 °C samples beyond TEAOH-2.0-2.0@200 and TEAOH-2.0-1.8@200 having distinctly higher crystallinity and AEI phase. For samples with a lower crystallization temperature crystallinity is lowered. For samples with TEAOH and CuO, lowering both the H_3PO_4 and TEAOH contents gave little to no crystalline phase. The two samples with high H_3PO_4 to TEAOH ratio (TEAOH-Cu-2.2-1.8 and TEAOH-Cu-2.0-1.6) gave AEI phase.

Table 4.4: Apparent phase, maxiumum height and calcuated SFR from XRD of samples synthesised varying H_3PO_4 and TEAOH content, with and without copper and at 150 or 200 °C. Inter refers to AEI/CHA-intergrowth and is assigned to $0.4 \leq$ SFR ≤ 0.7, AEI and CHA are assigned by SFR ≥ 0.8 and SFR ≤ 0.3 respectively. Samples which successfully gave AEI phase are highlighted.

Sample	CuO	Phase	Height	SFR
TEAOH-2.2-2.2@200	—	Inter	1679	0.4
TEAOH-2.0-2.2@200	—	Inter	1376	0.5
TEAOH-2.2-2.0@200	—	AEI	2344	0.96
TEAOH-2.0-2.0@200	—	AEI	6305	0.94
TEAOH-1.8-2.0@200	—	Inter	1503	0.4
TEAOH-2.0-1.8@200	—	AEI	5967	0.94
TEAOH-1.8-1.8@200	—	Inter	1838	0.4
TEAOH-1.6-1.8@200	—	AEI	4522	0.8
TEAOH-1.6-1.6@200	—	AEI	2978	0.9
TEAOH-2.2-2.0@150	—	AEI	2661	0.96
TEAOH-2.0-2.0@150	—	None	328	—
TEAOH-2.2-1.8@150	—	AEI	4339	0.96
TEAOH-2.0-1.8@150	—	AEI	2055	0.96
TEAOH-Cu-2.2-2.0	0.053	CHA	1136	0.3
TEAOH-Cu-2.2-1.8	0.051	AEI	1728	0.9
TEAOH-Cu-2.0-1.8	0.054	Inter	730	0.4
TEAOH-Cu-1.6-1.8	0.053	None	283	—
TEAOH-Cu-1.85-1.65	0.064	None	499	—
TEAOH-Cu-1.6-1.7	0.050	None	477	—
TEAOH-Cu-2.0-1.6	0.050	AEI	1600	0.9

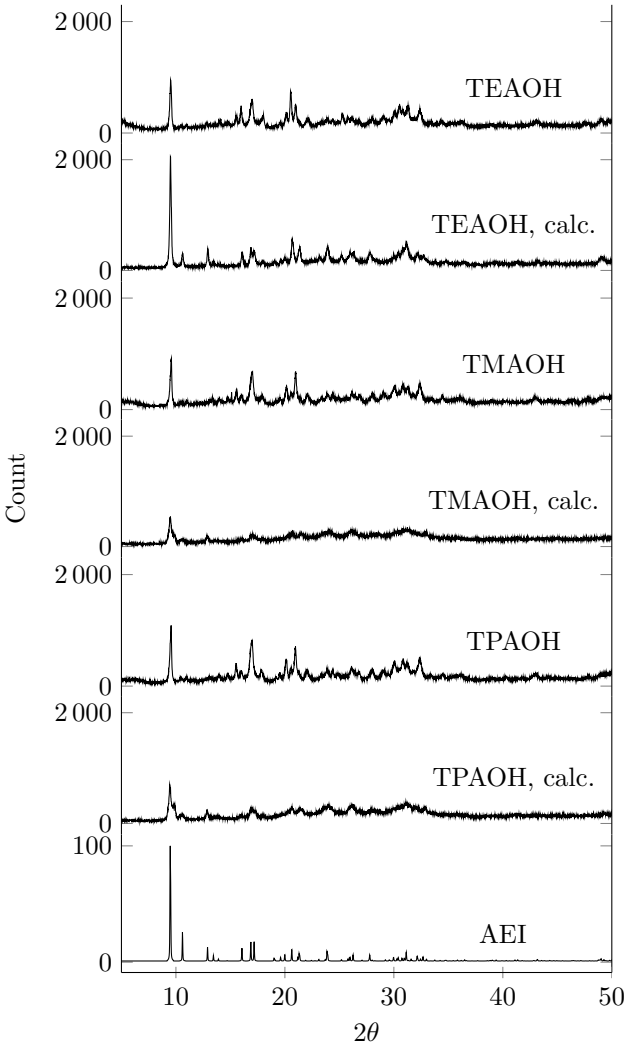

Figure 4.10: XRD patterns of samples synthesised using small amounts of TMAOH or TPAOH, see text. Reference TEAOH sample is sample TEAOH-2.0-1.8@150. "calc." refers to calcination at 550°C for 6h.

4.3 BET

To verify the microporosity of samples BET was employed. BET surface areas, micropore and external surface area for tested samples are shown in Figure 4.11 and given in Table 4.5. SAPO-18 is typically reported[8,74] to have a surface area around $650\,m^2\,g^{-1}$–$700\,m^2\,g^{-1}$. Samples DIPEA-Ref-8d and TEAOH-2.0-1.8@200 show a similar surface area ($533\,m^2\,g^{-1}$ and $457\,m^2\,g^{-1}$), but which are lower than areas previously reported. Sample without copper, but with lowered crystallization temperature (TEAOH-2.0-1.8@150) has a further lowered surface area, but sample which contains copper (TEAOH-Cu-2.0-1.6) has a very similar surface area. TEAOH-Cu-2.0-1.8 which also contains copper, but for which metallic copper is observed has a yet further lowered surface area. As all samples tested, other than TEAOH-2.0-1.8@200, has an external surface area $\sim 50\,m^2\,g^{-1}$ and so the changes in surface corresponds to changes in microporosity. From this it is clear that crystallization temperature and presence of metallic particles affect the microporosity, and the presence of copper alone does not majorly affect it.

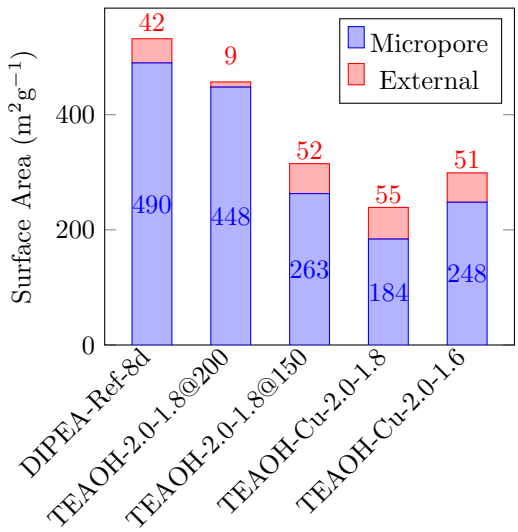

Figure 4.11: BET micro and external surface areas for select samples.

Table 4.5: BET surface, micropore and external surface area for select samples. All areas given in $m^2\,g^{-1}$.

Sample	Surface Area	Micropore Area	External Area
DIPEA-Ref-8d	533 ± 18	490	42
TEAOH-2.0-1.8@200	457 ± 16	448	9
TEAOH-2.0-1.8@150	315 ± 10	263	52
TEAOH-Cu-2.0-1.8	239 ± 7	184	55
TEAOH-Cu-2.0-1.6	299 ± 9	248	51

4.4 ICP-MS

The elemental composition of obtained samples was determined by ICP-MS. Sample composition given as molar ratio relative to Al is given in Table 4.6. The P/Al content is ∼0.9 for samples crystallized at 200 °C and lowered for samples crystallized at 150 °C (∼0.8). Si and Cu are retained approximately 1:1 into the solid relative to gel composition (Figure 4.12). As there is no clear change in composition from the presence of copper this can't be used to indicate the substitution (neither whether copper substitutes nor what element it substitutes with).

The P/Al and Si/Al ratios for DIPEA-Ref-8d-IE are lower than for DIPEA-Ref-8d meaning those elements were lost during ion-exchange. DIPEA-Ref-8d-IE has about 6 times more Si than TEAOH-2.0-1.8@200-IE, but contained only about 3 times more copper. This indicates a possible discrepancy between the Si content and the ion-exchange capacity.

Table 4.6: Sample composition relative to Al for select samples found by ICP-MS. Fraction of Cu in sample is also given.

Sample	Al	P	Si	Cu	wt% Cu
DIPEA-Ref-8d	1.0	0.82	0.21	—	—
DIPEA-TEPA-Cu-16d	1.0	0.61	0.24	0.050	2.4
TEAOH-2.0-1.8@150	1.0	0.79	0.040	—	—
TEAOH-2.0-1.8@200	1.0	0.92	0.027	—	—
TEAOH-1.8-2.0@200	1.0	0.86	0.051	—	—
TEAOH-2.0-2.0@200	1.0	0.91	0.029	—	—
TEAOH-2.2-2.0@200	1.0	0.90	0.045	—	—
TEAOH-Cu-2.0-1.8	1.0	0.78	0.037	0.034	1.4
TEAOH-Cu-2.0-1.6	1.0	0.81	0.030	0.038	1.8
DIPEA-Ref-8d-IE	1.0	0.73	0.198	0.017	0.90
TEAOH-2.0-1.8@200-IE	1.0	0.84	0.031	0.006	0.35

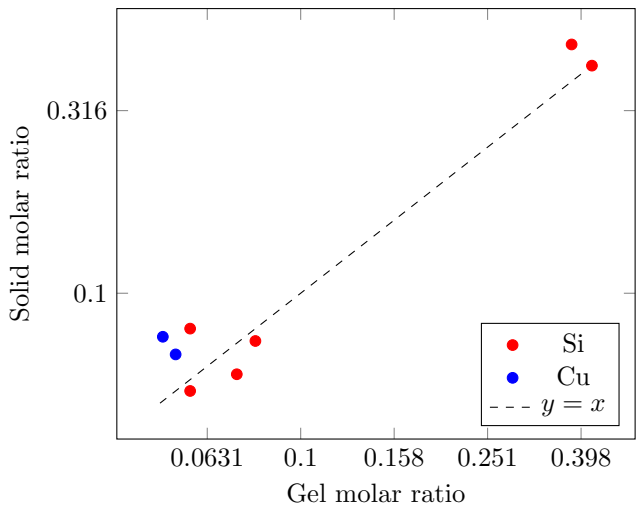

Figure 4.12: Molar ratio of Si and Cu relative to Al in obtained solid samples as a function of their hypothetical gel ratios.

4.5 FT-IR

FT-IR has been used to try to obtain evidence for the incorporation of copper in sample TEAOH-Cu-2.0-1.6. In particular, if a band corresponding to a Brønsted acid group which is not found for samples without copper (likely in the 3650–3400 cm^{-1} range), but which can be found for the sample with, this could be evidence for copper being incorporated as a T atom in the framework. Samples DIPEA-Ref-8d and TEAOH-2.0-1.8@150 has therefore been analysed for reference. Qualitative band sizes for all three samples are summarised in Table 4.7.

For sample DIPEA-Ref-8d (Figure 4.13) three small bands (3794, 3743, and 3680 cm^{-1}) corresponding to surface groups (Al–OH, Si–OH, P–OH) are visible and show no major change with CO pressure. A large band (3628 cm^{-1}) corresponding to Brønsted acid sites in cages is observable with a small contribution from acid sites in D6R units present as a shoulder (3606 cm^{-1}) on the larger band. Both of these red-shifts by ∼283 cm^{-1} with increasing CO pressure. The

Table 4.7: Magnitude of bands for plain, low Si, and copper containing SAPO-18 (samples DIPEA-Ref-8d, TEAOH-2.0-1.8@150, and TEAOH-Cu-2.0-1.6 respectively).

ν (cm^{-1})	3794	3774	3743	3680
Group	Al–$OH_{surface}$		Si–$OH_{surface}$	P–$OH_{surface}$
Plain[a]	Small	—	Small	Small
Low Si[b]	Small	Small	Small	Medium
Copper cont.[c]	Small	Small	Small	Medium

ν (cm^{-1})	3628	3606	3515	3352
Group	cage[d]	D6R[d]	Si–$OH_{surface+CO}$	cage/D6R[d]+CO
Plain[a]	Large	Small	Small	Large
Low Si[b]	Small	—	Small	Small
Copper cont.[c]	Small	—	Small	Small

ν (cm^{-1})	2175	2160	2140	2125
Group	CO_{acid}	$CO_{surface}$	CO_{free}	CO_{Cu}
Plain[a]	Large	—	Small	—
Low Si[b]	—	Large	Small	Small
Copper cont.[c]	—	Large	Small	Medium

[a]Sample DIPEA-Ref-8d
[b]Sample TEAOH-2.0-1.8@150
[c]Sample TEAOH-Cu-2.0-1.6
[d]Brønsted acid group; Al–OH–Si, located in the specified place.

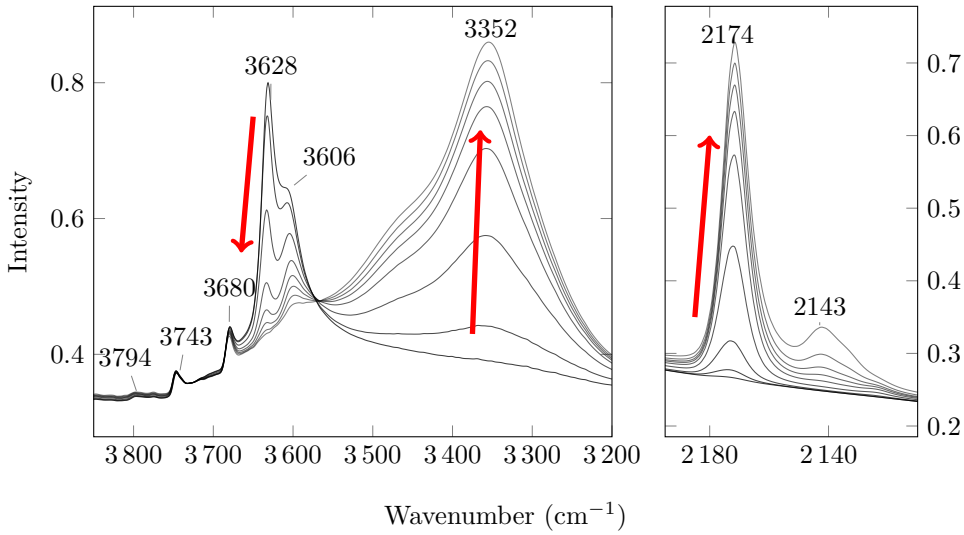

Figure 4.13: FTIR spectrum of DIPEA-Ref-8d. Red arrows inticate the direction of change with increasing CO pressure. Spectra taken at CO pressures 9.3, 15, 23, 33, 42, 51, 66, 96 µbar.

two bands are not distinguishable once shifted due to broadness of this band. A small shoulder at 3515 cm^{-1} is discernible at higher pressures corresponding to the P–OH red-shifting by ∼166 cm^{-1}. Similarly for higher pressures a band at 2140 cm^{-1} corresponding to free or physisorbed CO becomes present. This indicates that all groups with a high preference for CO have been probed. A large band at 2174 cm^{-1} grows with CO pressure. It can be assigned to CO adsorbed on acid groups and the maximum red-shifts slightly with CO pressure due to pore filling and multilayer adsorption.[63]

Sample TEAOH-2.0-1.8@150 (Figure 4.14) shows the same features with a few differences. An additional small band is present at 3774 cm^{-1} which is assignable as an additional Al–OH band.[7] The P–OH band at 3680 cm^{-1} is larger relative to other bands, in particular as the Brønsted acid groups (3628 cm^{-1} and 3606 cm^{-1}) being much smaller, the latter being not distinctly detectable. The same red-shift (∼283 cm^{-1}) occurs with increasing CO pressure indicating that similar, if fewer, acid groups are present in TEAOH-2.0-1.8@150 as in DIPEA-Ref-8d. The large band at 2175 cm^{-1} for DIPEA-Ref-8d is shifted to 2165 cm^{-1} for TEAOH-2.0-1.8@150. This shift can be assigned to adsorption onto surface groups. Two bands are present for TEAOH-2.0-1.8@150 and not for DIPEA-Ref-8d at 2150 and 2120 cm^{-1}. Bands at these wave-numbers is assigned to CO adsorption onto

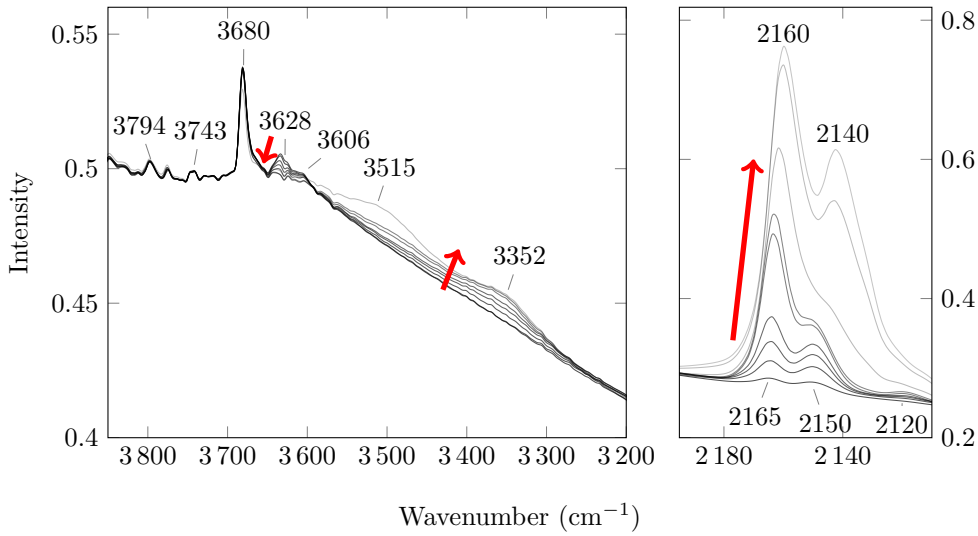

Figure 4.14: FTIR spectrum of TEAOH-2.0-1.8@150. Red arrows inticate the direction of change with increasing CO pressure. Spectra taken at CO pressures 18, 26, 35, 44, 97, 120, 770 µbar.

Cu^{2+} and Cu^{+} respectively.

The spectrum of TEAOH-Cu-2.0-1.6 (Figure 4.15) is similar to that of TEAOH-2.0-1.8@150. It possesses the same four bands from surface groups (Al–OH: 3794, 3774 cm^{-1}; Si–OH: 3743 cm^{-1}; P–OH: 3680 cm^{-1}), with the 3774 cm^{-1} band being slightly larger. Similarly the Brønsted acid bands (3628 cm^{-1}; the 3606 cm^{-1} band not distinguishable) are very low and shift by ∼283 cm^{-1}. No bands which can be attributed to Brønsted acid groups from copper are detected. The same band at 2160 cm^{-1} is also observed with increasing CO pressure for this sample. The notable features of the TEAOH-Cu-2.0-1.6 spectra compared to that of TEAOH-2.0-1.8@150 is the absence of a band at 2150 cm^{-1} (assigned to CO on Cu^{2+}) and that the band at 2122 cm^{-1} (CO on Cu^{+}) is much larger. This latter band could not be fully removed, even at prolonged evacuation. For these lower pressures though, the 2122 cm^{-1} band is revealed to consist of several bands (2130 cm^{-1} and lower), but these are not well separated from each other and are still assigned as CO adsorbed onto Cu^{+}.[65] As no copper induced Brønsted acid sites can be detected, but CO is adsorbed onto copper, these investigations indicate that copper is not framework incorporated in TEAOH-Cu-2.0-1.6.

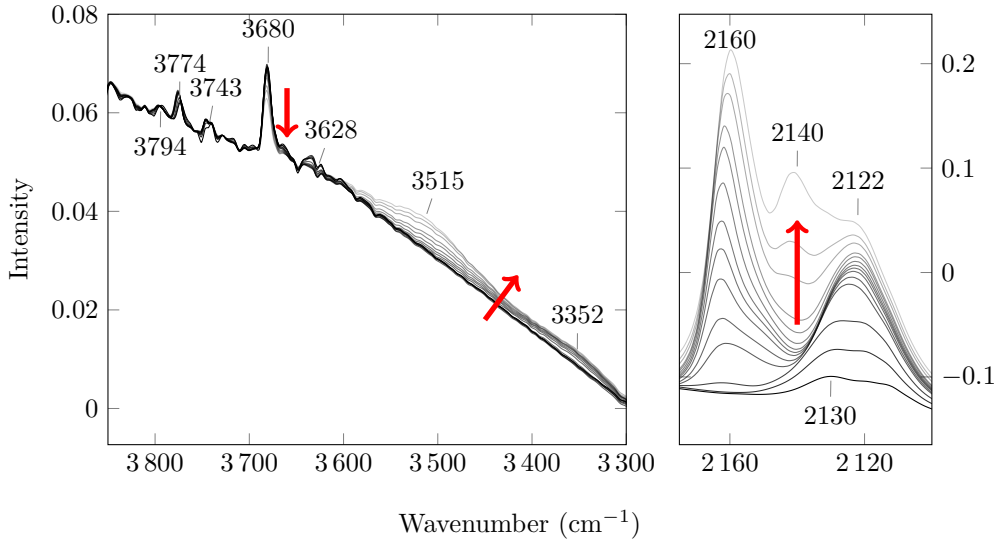

Figure 4.15: FTIR spectrum of TEAOH-Cu-2.0-1.6. Red arrows inticate the direction of change with increasing CO pressure. Spectra taken at CO pressures 0.8, 5.1, 10, 26, 35, 46, 56, 72, 97, 140, 210, 440, 650, 1400 µbar.

4.6 SCR of NOx

Sample TEAOH-Cu-2.0-1.6 was tested in HC-SCR in an effort obtain insight into the presence and availability of copper. SAPO-18 samples which were; not modified, ion-exchanged with Cu^{2+}, and mixed with CuO were tested for reference. Catalysis experiments first required checking the operability of the setup, with particular regard to the concentration of reactant gass (NO) decreasing over the course of an experiment.

The obtained NO_x concentrations for two blank runs (A and B) are given in appendix (Figure C.1). The concentration over time, $y(t)$ was fitted to functions of the form:

$$y(t) = c_0 + c_1 e^{-c_2 \cdot t} \tag{4.1}$$

For both of the runs the functions fitted to bypass and reactor measurements were virtually identical (parameters given in appendix; Table C.1). However the two runs show different functions. The residuals for each run (appendix; Figure C.2) show no clear pattern between them, with a maximal variance within 10 ppm. A 10 ppm difference is approximately equivalent to 0.5% conversion.

Conversion as a function of temperature for all samples is given in Figure 4.16.

Table 4.8: Mass and copper fraction of samples used for SCR of NO_x. Sample colour before and after reaction are also given. X_{500} is the conversion at 500 °C.

Sample	Mass (mg)	Cu wt%	Colour Before	Colour After	X_{500} %
DIPEA-Ref-8d	144.4	—	White	Beige	1.8
DIPEA-Ref-8d-IE	108.3	0.90	Blue	Brown	20.8
TEAOH-2.0-1.8@200-IE	50.8 [a]	0.35	Pale Blue	Beige	2.9
TEAOH-2.0-1.8@200-mix-CuO	78.0 [a]	4.7	Grey	Grey	3.8
TEAOH-Cu-2.0-1.6 (dry)	115.4	1.8	Green	Grey	12.1
TEAOH-Cu-2.0-1.6 (wet)	127.8	1.8	Green	Green	5.7

[a]Low mass used as there was insufficient sample remaining.

All samples show the same profile with a maximum conversion at 500 °C and generally having half that activity by 425 °C. There are two minor exceptions to this profile, which is the non-modified and the sample mixed with CuO. The latter has a slower decline until 450 °C before falling more rapidly and the former has a slight increase at lower temperature (<350 °C), but as this increase is less than 0.5% it is not significant. The generally obtained profile is similar to that found by Jakobsen[72] for ion-exchanged SAPO-34. The activity of the samples increase as DIPEA-Ref-8d-IE (20.8%) > TEAOH-Cu-2.0-1.6 (dry; 12.1%) > TEAOH-Cu-2.0-1.6 (wet; 5.7%) > TEAOH-2.0-1.8@200-mix-CuO (3.8%) > TEAOH-2.0-1.8@200-IE (2.9%) > DIPEA-Ref-8d (1.8%). Relative to copper content (Figure 4.17), the two ion-exchanged samples are quite close in activity. The activity of TEAOH-Cu-2.0-1.6 is between that of ion-exchanged and mixed samples. This suggests copper is either a mix of those two states or a distinct separate one (or a mix of all three).

Catalyst masses and colour are given in Table 4.8. Plain and ion-exchanged samples turned beige or brown over the course of reaction. For sample including mixed oxide and TEAOH-Cu-2.0-1.6 no change in colour was observed when running in wet feed, however it went from green to grey when running in dry feed. This suggests the copper species in TEAOH-Cu-2.0-1.6 has a higher hydrothermal stability than ones in ion-exchanged samples. No investigation were made on post-catalysis samples.

The activity of all samples tested is much lower than that previously reported[12,13,42,43,70–72] for copper containing SAPO-18/34.

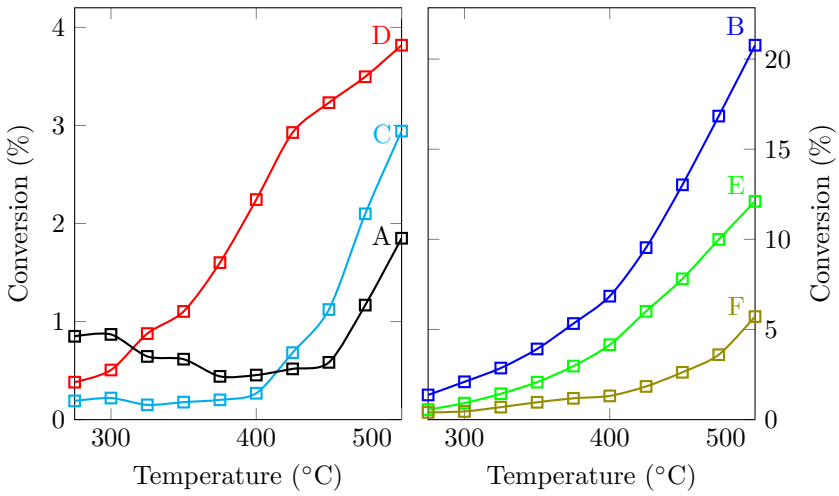

Figure 4.16: Conversion as a function of temperature for SCR of NO_x over select samples. Unless otherwise specified samples are run in wet feed. A DIPEA-Ref-8d, B DIPEA-Ref-8d-IE, C TEAOH-2.0-1.8@200-IE, D TEAOH-2.0-1.8@200-mix-CuO, E TEAOH-Cu-2.0-1.6 (dry), F TEAOH-Cu-2.0-1.6 (wet).

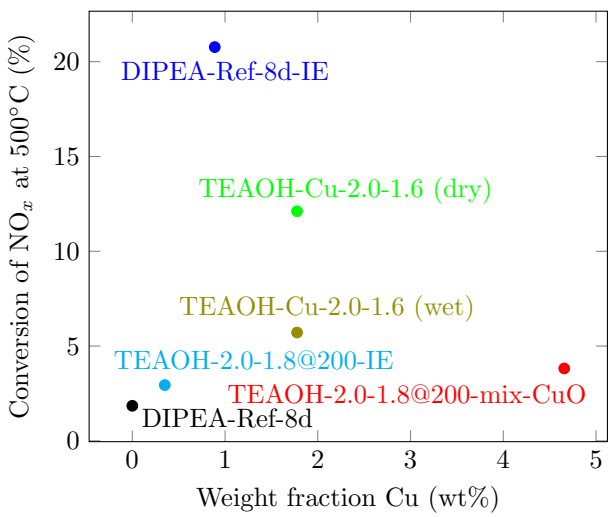

Figure 4.17: Conversion at 500 °C against fraction of Cu in the sample. Unless otherwise specified samples are run in wet feed.

Chapter 5

Discussion

The main goal of this work was synthesis of copper-incorporated SAPO-18. To that end, first a synthesis path for SAPO-18 using TEAOH was found necessary and using this path a candidate to be CuSAPO-18 was produced. The synthesis path and variables found to be important for the synthesis of CuSAPO-18 is discussed first (Section 5.1), before the success of copper incorporation in the obtained candidate is discussed (Section 5.2).

5.1 Development of synthesis path

Synthesis using DIPEA readily gave SAPO-18. However, copper in the presence of DIPEA reduces to metallic state. It can do so even when complexed with TEPA. This result differs to that of Martínez-Franco et al.[12] who did not observe any formation of metallic copper, but did instead observe copper situated in the same locations as that obtained by ion-exchange. The reduction of copper to metallic in the presence of DIPEA is hardly surprising. Moen and Nicholson[25] reported over 20 years ago that tertiary amines reduce copper, however use of complexing agents are purported to prevent such reduction.[12] It may appear that synthesis conditions have more impact on in method than what is apparent from literature. It is however not clear what may have caused the difference in results.

There was initially a goal to produce hierarchical SAPO-18 with copper. To that end samples were synthesised using DIPEA and PEG. Based on XRD findings this gives SAPO-18, however when TEPA and Copper is added the formed phase is different and notably not thermally stable. This shows TEPA can affect what phase is formed which is similar to the findings of Turrina et al.[47] Further tests were not performed due to time limitations.

On the back of these two findings, TEAOH was investigated as a template for

Table 5.1: Overview of parameters used to obtain sample which is the best candidate herein to be CuSAPO-18 (Sample TEAOH-Cu-2.0-1.6). Reactant contents are given as gel ratio relative to Al_2O_3.

Parameter	Value used	Comment
H_3PO_4	2	Could possibly be varied. If so the H_3PO_4/TEAOH ratio is likely important.
SiO_2	0.07	Not studied herein. Reported critical by Wendelbo et al.[1] Too high Si gives CHA.
CuO	0.050	Not varied herein.
Template	TEAOH	Use of TEAOH rather than DIPEA found necessary.
Template content	1.6	Lowest value tested. Higher values gave (partial) reduction of copper to metallic state.
H_2O	38	Found vital. All samples with water content above 50 gave CHA.
Cryst. T	150 °C	Not studied herein, but lowered temperature is reported important for copper in hydrothermal synthesis.[25]
Cryst. t	8 d	Not studied herein.
Ageing	*	TEAOH solution added prior to ageing.

SAPO-18. This has been previously reported, but much more rarely than with DIPEA. SAPO-18 was obtainable with TEAOH by using the ratio of Wendelbo et al.[1] An important difference between that work and this is that they used aluminium isopropoxide versus the pseudobohemite used herein. They also employed a filtering method to remove water after ageing, similar to that investigated herein. Whereas they obtained SAPO-18 with that method, our product was not distinctly so. It was instead found that removing water by heating the gel and letting water evaporate gave SAPO-18. Similarly, simply adding TEAOH prior to ageing gave SAPO-18. This last method is convenient as it has a minimal number and simple steps, with the only critical step being ensuring proper mixing of the viscous gel with TEAOH solution. Therefore that method was chosen for further investigations.

When then varying the H_3PO_4 and TEAOH content there was no pattern observed for what phase was obtained. It is possible that there is some unknown variable, or variables, which has not been controlled and which affects the

formed phase, but there is unfortunately little which can be learned from the set obtained herein. For such variations made with copper in the gel, it might be notable that samples where both H_3PO_4 and TEAOH contents were decreased gave no crystalline phase. Samples without copper did produce AEI with similar ratios. However when H_3PO_4 content was held constant or increased slightly, either SAPO-18, -34, or an intergrowth thereof was formed. There are unfortunately too few samples to say anything else succinct about this set. For all those samples (except one) metallic copper was observed upon opening the gel. The particularly notable thing in the synthesis of this sample (parameters of which is summarized in Table 5.1) is that it had the greatest H_3PO_4/TEAOH ratio (1.25) of samples made with copper. It is this sample which has been tested for copper incorporation, as discussed in Section 5.2.

Beyond the H_3PO_4 and TEAOH contents, a few other the parameters deserve a mention. Firstly the Si content, which has not been varied herein, but for which values < 0.1 have given SAPO-18. Secondly the water content which, as discussed above, appears critical for the formation of SAPO-18. Water content below 50 (molar ratio relative to Al_2O_3) was necessary for the formation of SAPO-18. The crystallization time was not studied for TEAOH synthesis. If the lowered surface area found for samples crystallized at a lower temperature (150 °C) is caused by incomplete crystallization, increasing the time could be a way to improve the resultant products. These findings correspond quite well with that of previous literature.[1,9,53] In particular the lowered TEAOH content is interesting. It is previously reported[9] to favour SAPO-18 over SAPO-34, and while such a trend could not be observed here, it might be valuable to future endeavours that the same variations (lowering the TEAOH content) is reported both to favour SAPO-18 formation as well diminish the formation of metallic copper.

5.2 Success of CuSAPO-18 synthesis

The main goal of this work was synthesis of SAPO-18 with framework incorporated copper. Fully incorporated copper should be tetrahedral and cause specific Brønsted acid sites (i.e. distinct from the sites caused by Si incorporation). The extent to which this was achieved is discussed here.

For all, except one (TEAOH-Cu-2.0-1.6), sample synthesised with TEAOH and CuO, metallic particles were observed alongside blue crystals. This one sample, along with other samples, was investigated using XRD, BET, ICP-MS, FT-IR and SCR of NO_x. It possessed similar crystallinity (1600 count versus 2000; arbitrary units) and surface area ($\sim$300 $m^2\,g^{-1}$) as samples with similar Si content and crystallization temperature. Both ICP-MS, FT-IR, and the green colour of the obtained sample shows that copper is present. Unfortunately, as green colour is reported for both tetrahedral[75] and tetragonally distorted octa-

hedral[38,41] coordinated copper, it can't reliably be used to indicate coordination.

FT-IR spectra of sample with and without copper (with same Si content) show very similar acid groups, with no Brønsted acid groups attributable to the presence of copper detected. This means copper is not shown to be framework incorporated by FT-IR. A more powerful technique such as X-ray adsorption (XANES, EXAFS; X-ray absorption near edge structure, Extended X-ray absorption fine structure)[38] is needed to determine the actual coordination of copper. These methods where not available in time for the relevant sample.

Unfortunately, one of the reference materials (TEAOH-2.0-1.8@150) used in FT-IR also showed bands (2150 and 2120 cm^{-1}) which are attributed to the presence of copper. However, as the sample of interest (TEAOH-Cu-2.0-1.6) did not show the former of these and the latter was substantially larger, it is clear any copper present in the reference sample is in a different form. The most likely explanation for this is contamination of the sample used for reference at some point prior to FT-IR experiments, but it is not clear when this would have happened.

In SCR of NO_x the copper sample (i.e. the one containing copper from synthesis) showed an activity intermittent to that of ion-exchanged SAPO-18 and SAPO-18 mixed with CuO (5.7% maximum conversion versus 20.8% and 3.8% respectively). This suggests that either framework copper species are less active than or part of copper is present as copper metal/oxide, or both. If part of the copper is metallic/oxide, which of the two can't be determined. The green colour of sample was retained during reaction under wet feed. For dry feed the sample was grey after reaction, which is similar to reported framework copper by Nicholson and Nilsen.[40]

The conversion achieved in SCR is much lower than that obtained by other workers. Martínez-Franco et al.[12] reported almost 100% conversion for ion-exchanged and ion-exchange-like Cu-SAPO-18. Though notably their materials contained 2.5–6.2 wt% copper and they used NH_3 as a reductant and significantly less NO (500 ppm versus 2000 ppm used herein) in their experiments. Mathisen et al.[38] also achieved higher conversion (∼15%) with tetragonally-distorted octahedrally coordinated copper in SAPO-5 using comparable reaction to those herein. The notable exceptions to this is the absence of water in the feed and again a higher copper content (4.3–8.2% versus 1.8%). Adjusting for the 2–4-fold difference in copper content, the difference in conversion (15% versus 12% for dry feed) might be understandable. It is also worth noting that these other workers observed activity over a broad, and subsequently lower, range of temperatures whereas herein the activity fell rapidly with lower temperatures. The activity profile is similar to that obtained by Jakobsen[72] for a sample with a copper content of 1.4 wt%. While more research would be necessary to establish such a relation, it could be the activity profile is related to the amount of copper.

Chapter 6

Conclusion

In summary, the goal of isomorphously substituting copper into SAPO-18 was not achieved. Further investigation is necessary to determine the state of copper accurately, but present results indicate copper is not isomorphously substituted.

However the present work has obtained a synthesis route for SAPO-18 using TEAOH and have found a indication that lowering the amount of TEAOH allows for the formation of CuSAPO-18 where metallic copper is not observed. However the exact state of copper in this sample could not be determined. The so obtained material was less active for the selective catalytic reduction of NO_x than ion-exchanged samples and far less than previously reported materials.

The key findings of this work is the lowered TEAOH content being beneficial towards copper incorporation, the lowered water content being necessary towards SAPO-18 formation, and that rapid addition of template or evaporation of excess water can be used to compensate for the low water content of the gels. It may be worth emphasizing that the synthesis conditions presented herein are not optimized, but rather could provide a stepping stone and direction for future work.

Chapter 7

Future Work

The exact state of copper in the most promising sample could not be determined. Therefore future work directly relating to this one would be analysing the CuSAPO-18 sample (TEAOH-Cu-2.0-1.6) using a more powerful technique, i.e. X-ray spectroscopy (XANES, EXAFS), to hopefully establish such nature. Once our group has the instrument time to perform such experiments, this sample could be tested.

More broadly future endeavours to incorporate copper into SAPO-18 should focus on further lowered TEAOH content (> 1.6) and increased H_3PO_4/TEAOH ratio (> 1.25). Similarly the quality, in particular microporosity, of such SAPO-18 can in all likelihood be improved. The most likely candidates towards achieving such improvement is increasing the crystallization time, and possibly the use of evaporation to remove added water after gel ageing. It would likely also be interesting for future works to investigate the possibility, and effect of, increased copper content in the gels and subsequently in the obtained materials. Increasing the copper content would in particular be interesting to catalytic applications (i.e. HC-SCR). Similarly, investigating the incorporation of copper into hierarchical SAPO-18 would be relevant to such purposed. However improving the synthesis with regards to crystallinity and microporosity should likely be prioritized ahead of introducing mesopores.

Bibliography

(1) Wendelbo, R. et al. *Applied Catalysis A: General* **1996**, *142*, L197–L207.

(2) Wilson, S. T. et al. *Journal of the American Chemical Society* **1982**, *104*, 1146–1147.

(3) Lok, B. M. et al. *Journal of the American Chemical Society* **1984**, *106*, 6092–6093.

(4) Bond, G. C. et al. *Journal of the Chemical Society, Chemical Communications* **1985**, 1056–1057.

(5) Parise, J. B. *Inorganic Chemistry* **1985**, *24*, 4312–4316.

(6) Van Heyden, H. et al. *Chemistry of Materials* **2008**, *20*, 2956–2963.

(7) Chen, J.; Thomas, J. M. *Journal of the Chemical Society, Chemical Communications* **1994**, 603–604.

(8) Nazari, M. et al. *Journal of Porous Materials* **2016**, *23*, 1037–1046.

(9) Wang, Y. et al. *RSC Advances* **2016**, *6*, 104985–104994.

(10) Ateka, A. et al. *International Journal of Hydrogen Energy* **2016**, *41*, 18015–18026.

(11) Cortés-Reyes, M. et al. *Microporous and Mesoporous Materials* **2017**, *241*, 258–265.

(12) Martínez-Franco, R. et al. *Journal of Catalysis* **2014**, *319*, 36–43.

(13) Chen, Z. et al. *Chemical Engineering Journal* **2018**, *348*, 608–617.

(14) Richter, M. et al. *Applied Catalysis B: Environmental* **2007**, *73*, 269–281.

(15) Chaloulakou, A. et al. *Atmospheric Environment* **2008**, *42*, 454–465.

(16) Gaffney, J. S. et al. *Environmental science & technology* **1987**, *21*, 519–524.

(17) Agency, E. E. *European Union emission inventory report 1990-2016*; tech. rep. 6; EU, 2018, pp 48–53.

(18) IZA Structure Commision. http://www.iza-structure.org/IZA-SC_FTC.htm. Published 18.8.17. Read 01.03.18.

(19) Ashtekar, S. et al. *The Journal of Physical Chemistry* **1994**, *98*, 4878–4883.

(20) Tan, J. et al. *Microporous and Mesoporous Materials* **2002**, *53*, 97–108.

(21) Chen, J. et al. *The Journal of Physical Chemistry* **1994**, *98*, 10216–10224.

(22) Fan, D. et al. *Journal of Materials Chemistry* **2012**, *22*, 6568–6574.

(23) Francis, R. J.; O'Hare, D. *Journal of the Chemical Society, Dalton Transactions* **1998**, 3133–3148.

(24) Ferey, G. et al. *Chemistry of Materials* **2013**, *26*, 299–309.

(25) Moen, A.; Nicholson, D. G. *Journal of the Chemical Society, Faraday Transactions* **1995**, *91*, 3529–3535.

(26) Hartmann, M.; Kevan, L. *Chemical reviews* **1999**, *99*, 635–664.

(27) Ateka, A. et al. *Fuel processing technology* **2016**, *152*, 34–45.

(28) García-Trenco, A. et al. *Catalysis today* **2012**, *179*, 43–51.

(29) Naik, S. P. et al. *Industrial & Engineering Chemistry Research* **2008**, *47*, 9791–9794.

(30) Pluth, J. et al. *Materials Research Bulletin* **1977**, *12*, 1001–1007.

(31) Fickel, D. W.; Lobo, R. F. *The Journal of Physical Chemistry C* **2009**, *114*, 1633–1640.

(32) Frache, A. et al. *Topics in Catalysis* **2003**, *22*, 53–57.

(33) Akolekar, D. B. et al. *Journal of the Chemical Society, Faraday Transactions* **1998**, *94*, 155–160.

(34) Leistner, K.; Olsson, L. *Applied Catalysis B: Environmental* **2015**, *165*, 192–199.

(35) Xu, M. et al. *Applied Catalysis B: Environmental* **2018**, *220*, 161–170.

(36) Muñoz, T. et al. *The Journal of Physical Chemistry B* **1998**, *102*, 1379–1386.

(37) Lee, C. W. et al. *Zeolites* **1993**, *13*, 565–571.

(38) Mathisen, K. et al. *Journal of Materials Chemistry* **2005**, *15*, 204–217.

(39) Lee, J. D., *Concise Inorganic Chemistry*, 4th ed.; Chapman & Hall.

(40) Nicholson, D. G.; Nilsen, M. H. *Journal of Materials Chemistry* **2000**, *10*, 1965–1971.

(41) Kristiansen, T. et al. *The Journal of Physical Chemistry C* **2011**, *115*, 19260–19268.

(42) Sørli, G. Effect of Porosity on the Hydrothermal Stability of CuSAPO-34 for the deNOx Process., MA thesis, NTNU, 2016.

(43) Hutcheson, A. Effect of Porosity and Copper Content on Copper Containing SAPO-34 for Removal of NOx., MA thesis, NTNU, 2018.

(44) Snyder, B. E. et al. *Chemical reviews* **2017**, *118*, 2718–2768.

(45) Martín, N. et al. *Chemical communications* **2015**, *51*, 11030–11033.

(46) Liu, J. et al. *Chinese Journal of Catalysis* **2016**, *37*, 750–759.

(47) Turrina, A. et al. *Microporous and Mesoporous Materials* **2015**, *215*, 154–167.

(48) Chen, J. et al. *Catalysis letters* **1994**, *28*, 241–248.

(49) Baerlocher, C. et al., *Atlas of zeolite framework types*, 6th ed.; Elsevier: 2007.

(50) Shin, Y. H. et al. *Korean Journal of Chemical Engineering* **2018**, 1–8.

(51) Momma, K.; Izumi, F. *Journal of applied crystallography* **2011**, *44*, 1272–1276.

(52) Simmen, A. et al. *Zeolites* **1991**, *11*, 654–661.

(53) Smith, R. L. et al. *Chemistry of Materials* **2015**, *27*, 4205–4215.

(54) Sławiński, W. A. et al. *Microporous and Mesoporous Materials* **2014**, *195*, 311–318.

(55) Everett, D. *Pure and Applied Chemistry* **1972**, *31*, 577–638.

(56) Pérez-Ramírez, J. et al. *Chemical Society Reviews* **2008**, *37*, 2530–2542.

(57) O'Connell, K.; Regalbuto, J. R. *Catalysis Letters* **2015**, *145*, 777–783.

(58) Inoue, M. et al. *Chem. Commun.* **1999**, 957–958.

(59) Brunauer, S. et al. *Journal of the American chemical society* **1938**, *60*, 309–319.

(60) Sing, K. S. *Pure and applied chemistry* **1985**, *57*, 603–619.

(61) Thomas, R., *Practical guide to ICP-MS: a tutorial for beginners*; CRC press: 2013.

(62) Berthomieu, C.; Hienerwadel, R. *Photosynthesis research* **2009**, *101*, 157–170.

(63) Bordiga, S. et al. *The Journal of Physical Chemistry B* **2005**, *109*, 2779–2784.

(64) Zaki, M. I.; Knözlngem, H. *Spectrochimica Acta Part A: Molecular Spectroscopy* **1987**, *43*, 1455–1459.

(65) Hadjiivanov, K. I. et al. *Journal of the Chemical Society, Faraday Transactions* **1996**, *92*, 4595–4600.

(66) Wang, L. et al. *Journal of Catalysis* **2012**, *289*, 21–29.

(67) Yahiro, H.; Iwamoto, M. *Applied Catalysis A: General* **2001**, *222*, 163–181.

(68) Cheng, X.; Bi, X. T. *Particuology* **2014**, *16*, 1–18.

(69) Forzatti, P. *Applied catalysis A: general* **2001**, *222*, 221–236.

(70) Ishihara, T. et al. *Journal of Catalysis* **1997**, *169*, 93–102.

(71) Schjetlein, E.-M. M. Understanding the Effect of Porosity of Cu: SAPO-34 and AgCu: SAPO-34 for the HC-SCR deNOx Reaction., MA thesis, NTNU, 2018.

(72) Jakobsen, T. D. SAPO-34 with Copper: Investigation of hierarchical pore characteristics and interactions with copper for catalytic applications., MA thesis, Institutt for kjemi, 2014.

(73) Gan, F. et al. *Chemometrics and Intelligent Laboratory Systems* **2006**, *82*, 59–65.

(74) Kladis, C. et al. *Journal of Molecular Catalysis A: Chemical* **2003**, *203*, 193–202.

(75) Trouillet, L. et al. *Physical Chemistry Chemical Physics* **2000**, *2*, 2005–2014.

Appendix A

Additional XRD patterns

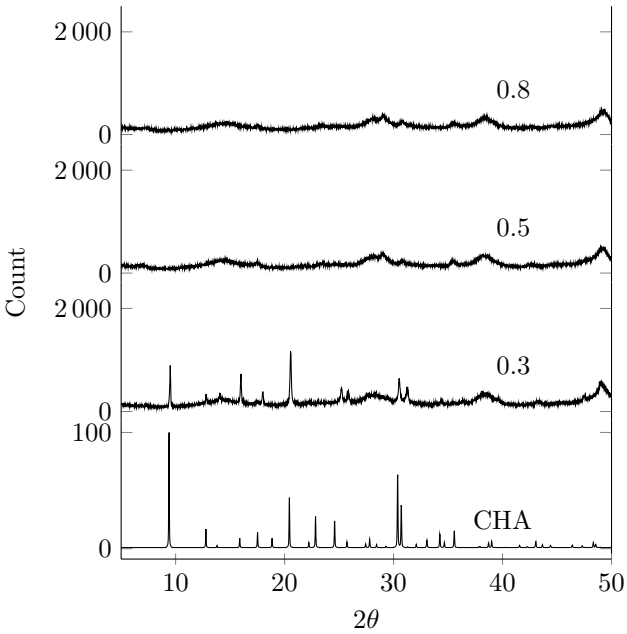

Figure A.1: XRD patterns for samples with H_3PO_4/Al molar ration of 0.7 and varying TEAOH/Al ratio.

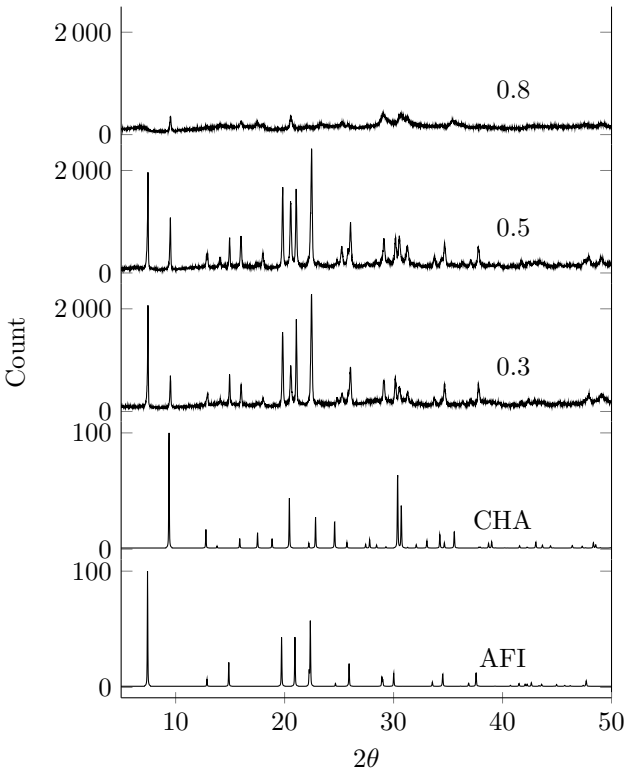

Figure A.2: XRD patterns for samples with H_3PO_4/Al molar ration of 1.2 and varying TEAOH/Al ratio.

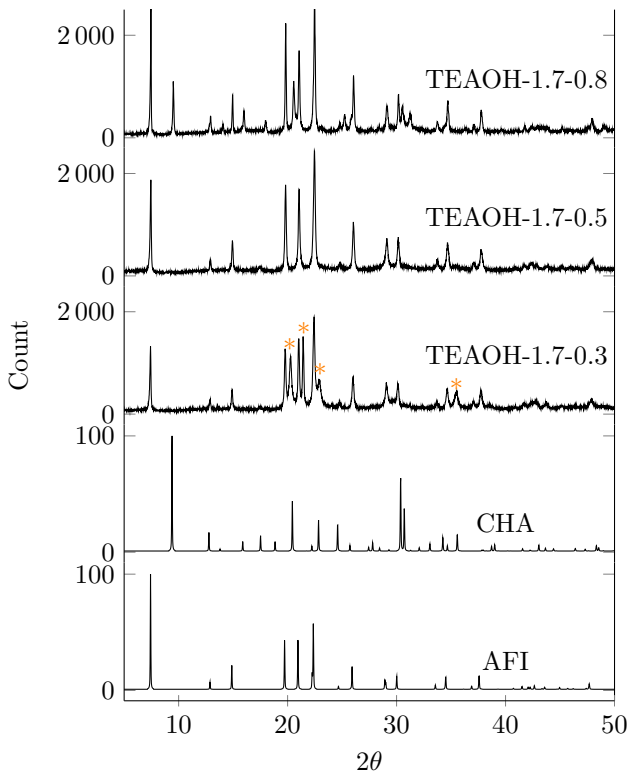

Figure A.3: XRD patterns for samples with H_3PO_4/Al molar ration of 1.7 and varying TEAOH/Al ratio.

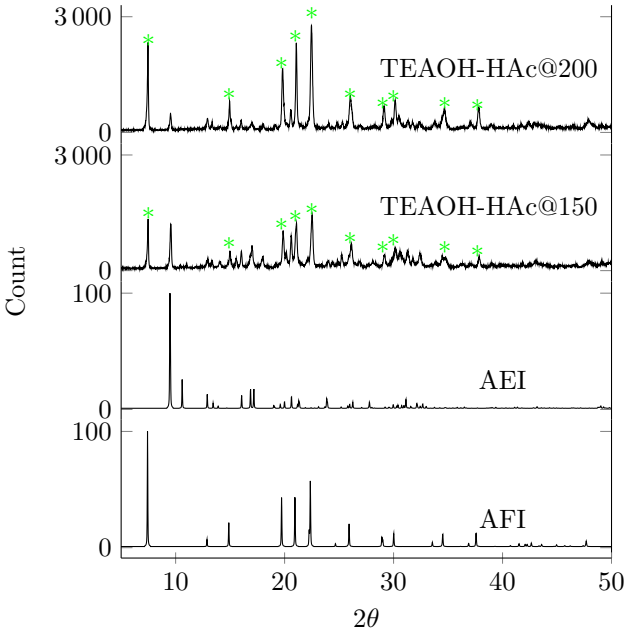

Figure A.4: XRD patterns of samples synthesised using TEAOH and HAc. Green stars mark AFI peaks.

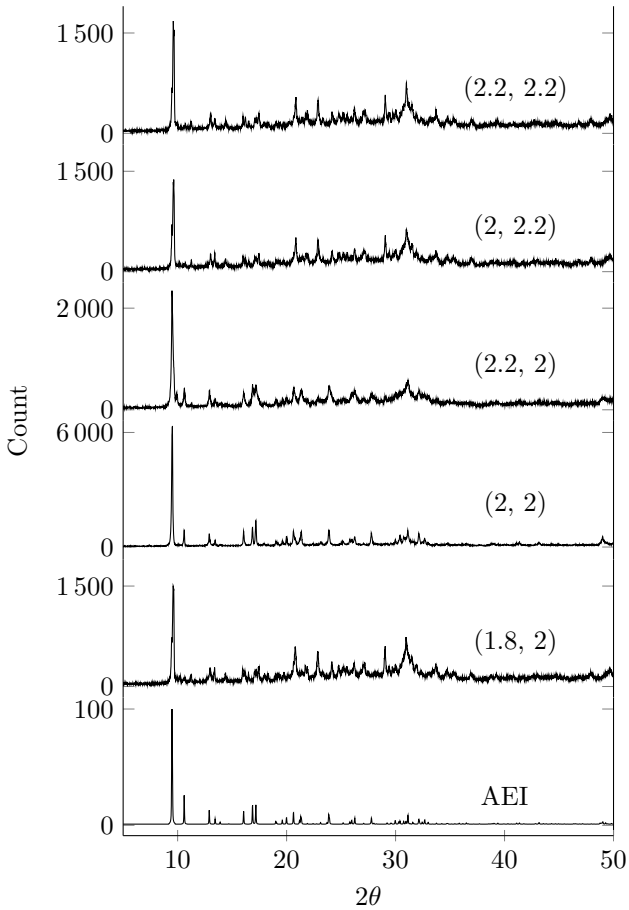

Figure A.5: XRD patterns of samples synthesized with varying (H_3PO_4, TEAOH) ratios and crystallized at 200 °C for 8 d. All samples calcined at 550 °C for 6 h.

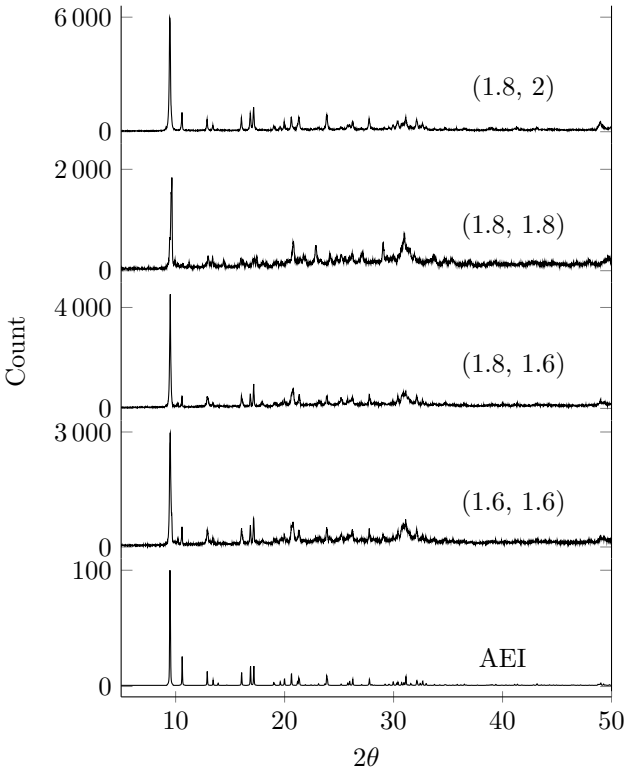

Figure A.6: Further XRD patterns of samples synthesized with varying (H_3PO_4, TEAOH) ratios and crystallized at 200 °C for 8 d. All samples calcined at 550 °C for 6 h.

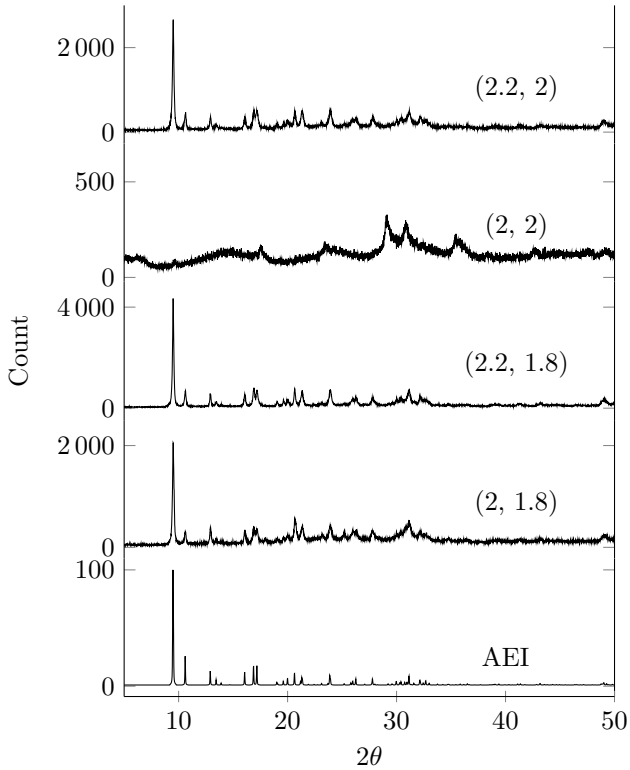

Figure A.7: XRD patterns of samples synthesized with varying (H_3PO_4, TEAOH) ratios and crystallized at 150 °C for 8 d. All samples calcined at 550 °C for 6 h.

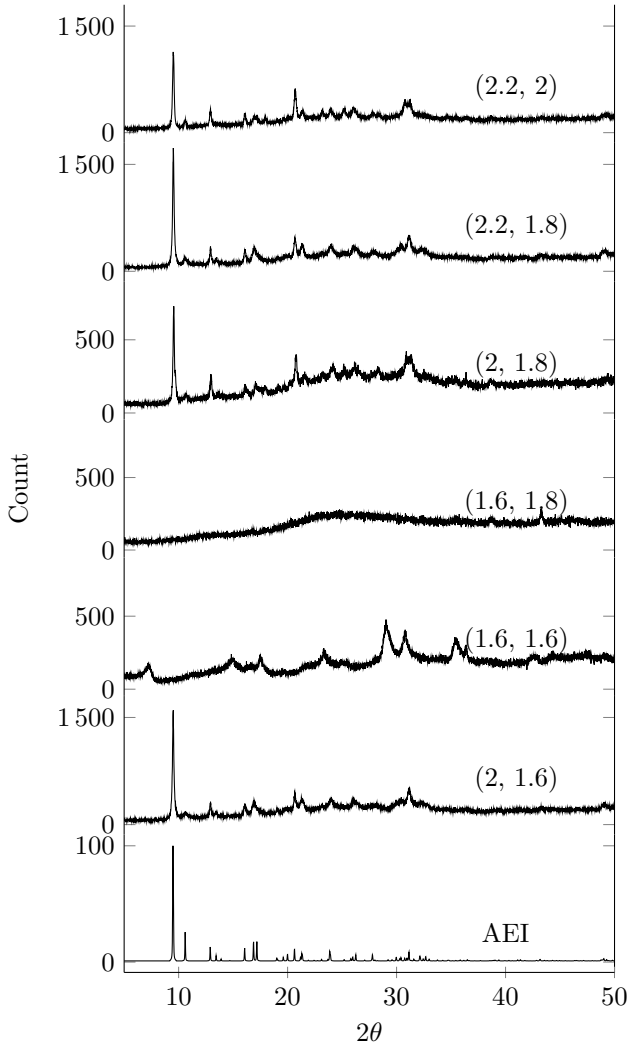

Figure A.8: XRD patterns of Cu containing samples synthesized with varying (H_3PO_4, TEAOH) ratios and crystallized at 150 °C for 8 d. All samples calcined at 550 °C for 6 h.

Appendix B

Additional BET Data

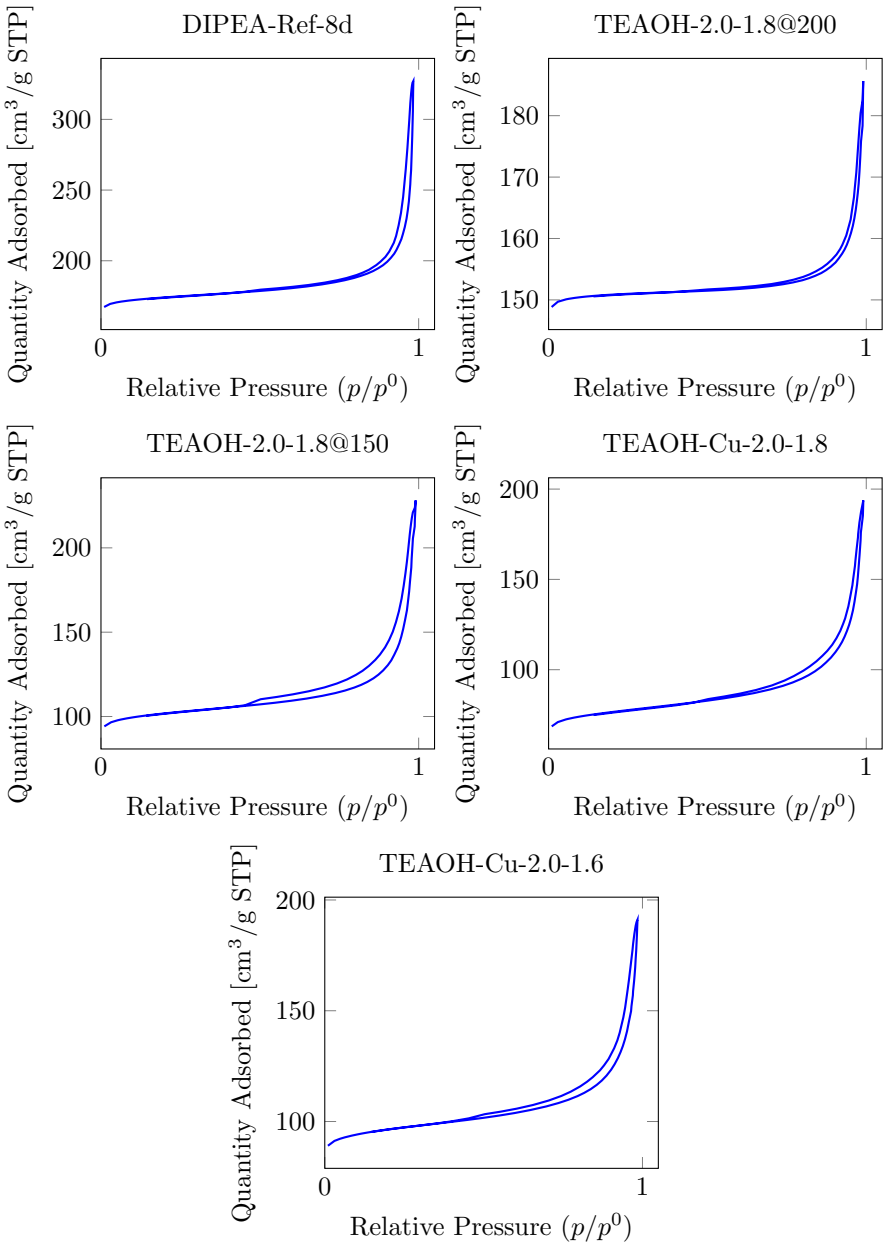

Figure B.1: BET adsorption plots.

Appendix C

Additional SCR Data

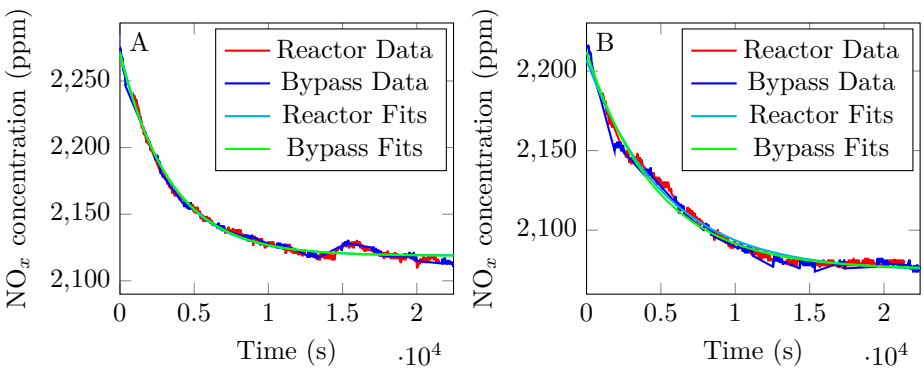

Figure C.1: NO_x concentration for two blank runs (A and B) over time.

Table C.1: Parameter values of functions of form of Equation 4.1.

Function	c_0	c_1	c_2
A Reactor	2119	153.2	3.00×10^{-4}
A Bypass	2118	151.5	2.92×10^{-4}
B Reactor	2074	132.9	1.91×10^{-4}
B Bypass	2075	136.8	2.13×10^{-4}

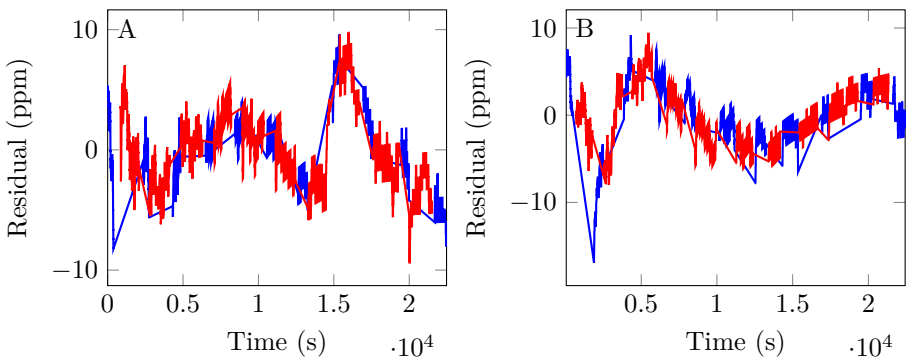

Figure C.2: Residuals of functions fitted to blank runs (A and B). Bypass and reactor measurements is given in blue and red respectively.

NTNU

Norwegian University of
Science and Technology